Particulate Matter Chemistry and Dynamics in the Twilight Zone at VERTIGO ALOHA and K2 Sites.

James K.B. Bishop[1,2] and T.J. Wood[2]

1. Department of Earth and Planetary Science, University of California, Berkeley, CA, 94720-4767, USA, tel 1-510-642-4110, email: jkbishop@berkeley.edu; Corresponding Author.

2. Earth Sciences Division, Lawrence Berkeley National Laboratory, Berkeley, CA 94720, USA tel. 1-510-486-4104, tjwood@lbl.gov

Key words: VERTIGO, Optics, Particulate Organic Matter, Opal, POC, PIC, flux, remineralization

Abstract.

Understanding particle dynamics in the 'Twilight Zone' is critical to prediction of the ocean's carbon cycle. As part of the VERTIGO (VERtical Transformations In the Global Ocean) project, this rarely sampled regime extending from the base of the euphotic layer to 1000 m, was characterized by double-paired day/night Multiple Unit Large Volume in-situ Filtration System (MULVFS) deployments and by ~100 high-frequency CTD / transmissometer / turbidity sensor profiles. VERTIGO studies lasting three weeks, contrasted oligotrophic station ALOHA (22.75°N 158°W), sampled in June – July 2004, with a biologically productive location (47°N 161°E) near station K2 in the Oyashio, occupied July – August 2005. Profiles of major and minor particulate components (C_{org}, N, P, Ca, Si, Sr, Ba, Mn) in <1, 1-51, and >51μm size fractions, in-water optics, neutrally buoyant sediment trap (NBST) fluxes, and zooplankton data were intercompared. MULVFS total C_{org} and C-Star particle beam attenuation coefficient (C_P) were

consistently related at both sites with a 27 μM m^{-1} conversion factor. At K2, C_P profiles further showed a multitude of transient spikes throughout the water column and spike abundance profiles closely paralleled the double peaked abundance profiles of zooplankton. Also at K2, copepods contributed ~40% and 10%, night and day, respectively to >51 μm C_{org} of MULVFS samples in the mixed layer, but few copepods were collected in deeper waters; however, non-swimming radiolarians were quantitatively sampled. A recent hypothesis regarding POC differences between pumps and bottles is examined in light of these results. Particulate >51 μm C_{org}, N, and P at both ALOHA and K2 showed strong attenuation with depth at both sites. Notable at ALOHA were unusually high levels of >51 μm Sr (up to 4 nM) in the mixed layer, a reflection of high abundances of $SrSO_4$ precipitating Acantharia. Notable at K2 were major changes in water column inventories of many particulate components to 700 m over 10 days. Carbon mass balance, with the consideration of particle inventory changes included, indicated that over 98% and 96% of primary produced C_{org} was remineralized shallower than 500 m at ALOHA and K2, respectively. Production of $CaCO_3$ was estimated to be ~0.06, 0.89 and 0.02 mmols m^{-2} d^{-1} at ALOHA and at K2 during two separate week long study periods, respectively. Similarly, Si production was estimated to be ~0.08, 10.7, and 4.2 mols m^{-2} d^{-1}. An estimated 50% and 65% of produced Si was remineralized by 500m at ALOHA and K2, respectively. Little carbonate dissolution was seen in the upper 500 m at ALOHA, a reflection of 400% super saturation of surface waters and the 700 m deep saturation horizon. Over 92% of produced $CaCO_3$ was dissolved shallower than 500 m at K2 and biological enhancement of dissolution was readily apparent in waters above the 200 m calcite saturation horizon.

1. Introduction

Biotic processes that form, change, transport, and remineralize particulate organic carbon, silicon, calcium carbonate, and other minor and trace chemical species in the water column are central to the ocean's geochemical cycling of elements and are of fundamental importance to the ocean carbon cycle (Broecker and Peng, 1982; Volk and Hoffert, 1985; Armstrong et al., 2002). These processes are fast and poorly observed in the upper kilometer of the ocean, and are rarely observed for periods of longer than several days at any location. The VERtical Transport In the Global Ocean (VERTIGO) project (Buesseler et al., 2008) provided an opportunity to follow particles from their production to sedimentation over two three-week-long summer time periods in two contrasting regimes: highly oligotrophic waters of station ALOHA (22.75°N 158°W; occupied June-July 2004), the site of the Hawaii Ocean Time Series program (Karl et al. 1996) and a site (at 47°N 161°E) one degree east of station K2; occupied July-August 2005), in biologically productive waters of the Oyashio (Fig. 1).

Our contribution to VERTIGO was three-fold: We quantified the high frequency variability of particulates using optical transmission and scattering sensors, we sampled large and small particles using the Multiple Unit Large Volume in-situ Filtration System (MULVFS; Bishop et al., 1985; Lam and Bishop, 2007) from the surface mixed layer through the "twilight zone" to 1000 m, and we deployed surface buoy-tethered optical sedimentation traps (buoy- OST) to capture the high frequency (hourly) variations of sedimentation.

This paper describes spatial and temporal variability and biological associations of major and minor particulate components C_{org}, N, P, Ca, Si, Sr, Ba, and Mn directly sampled during the paired day/night MULVFS deployments and the larger scales of particle variability in time and space established through the 20 times more frequent CTD/optical sensor casts. The buoy-OST results will be described elsewhere. There has been no description of major particulate phases inclusive of Ca and Si at either K2 or ALOHA.

We address five major questions: (1) How do concentrations of large and small particles sampled in-situ from the water column relate to contemporaneously measured particle fluxes at ALOHA and K2? (2) Is there evidence for shallow biologically mediated carbonate dissolution in supersaturated/near-saturated waters at ALOHA and K2? (3) How well can the VERTIGO water column at K2 be treated as a 1D (vertical) system for carbon transformation processes? In other words, are vertically acting biological processes dominant in explaining changes of biogenic particle distributions over time? (4) Are spikes seen in scattering sensor and transmissometer profiles a measure of aggregate particles or zooplankton? We further address a methodological question: (5) Are the recently reported differences (Liu et al., 2005; Gardner et al., 2003) in particulate C_{org} captured by bottles and in-situ pumps an artifact of zooplankton avoidance of in-situ pumps or an artifact of (a) loss of >51 μm particles from the pumps these investigators described and/or (b) an artifact of sample preservation?

2. Methods

2.1 Multiple Unit Large Volume in-situ Filtration System

MULVFS sampling and most other VERTIGO studies took place during two week-long intensive study periods (D1 and D2) at ALOHA (in 2004) and K2 (in 2005). ALOHA intensive studies took place from day 175 to 181 (D1) and from day 185 to 191 (D2); at K2, the intensive periods were days 211 to 218 (D1), and days 221 to 228 (D2).

We highlight VERTIGO sampling detail and enhancements to MULVFS since it was last described (Bishop et al., 1985). MULVFS consists of 12 ship-electricity powered pump units deployed simultaneously to kilometer depths using a dedicated (unified) 1000 m long electromechanical cable and winch system. MULVFS sample depths were 30, 55, 80, 105, 155, 205, 255, 330, 480, 575, 680, 770, and 880 m at ALOHA, and 10, 35, 60, 85, 135, 185, 235, 310, 460, 560, 660, 760, and 810 m at K2. The shallowest sample was always within the surface mixed layer. VERTIGO casts were timed to capture particles near local noon and midnight to investigate the effects of diurnal zooplankton migrations on particle distributions. At ALOHA, 3 day and 2 night casts were obtained; at K2, 2 day/night pairs were obtained (Tables 1 and 2).

Each pump unit can collect samples of particulate and dissolved species using three flow paths (Fig. 2A and B). Check and gas release (de bubbler) valves (Fig. 2B) protect filter samples from the effects of back flow, contamination, and disruption due to trapped air

on deployment and degassed air expansion on recovery. The later is a problem in shallow samples.

Depending on depth and particle concentration, 2000 to 16000 liter volumes of seawater are filtered under a suction of <0.8 atmospheres over four to five hours through the main multistage (3 anti-washout baffles and two filter stages) filter holder (Fig. 2C). The first anti-washout baffle (Fig. $2C_A$) is a heavy polyethylene plastic cover with incised 1 cm scale triangular flaps centered over each of the 52 tubes of the second baffle stage (Fig. $2C_B$) and was added to ensure particle retention under strong current shears.

The main filter series (with an effective filtration diameter of 24.5 cm) consists of a 51 μm polyester square weave mesh prefilter supported by 149 μm polyester mesh and 1.2 cm spaced 1.2 cm thick plastic grid in the prefilter stage, followed by two identical Whatman QMA quartz fiber filters supported by 149 μm polyester mesh and 149 μm porous polyethylene frit. All filters and components are acid cleaned. The three particle size fractions represented by prefilter and QMA filters are >51, 1-51, and '< 1' μm. Fiber filters are 'depth' filters and particles are captured from the flow by the fibers, not pores. Thus a second filter captures additional small particles that pass through the first (Bishop and Edmond, 1976). The '<1' μm fraction, thus represents some of particles in the larger sub micron particle class (Bishop et al., 1977, 1985).

The second flow path (Fig. 2A-2; 2B-2), with 500-2000 liter water flow capacity was used for separate multi-stage filter assemblies and in-line Mn radionuclide adsorption

cartridges (Charette et al., 1999). The filter assembly used by T. Trull (University of Tasmania, UTAS) is shown in Fig. 2A-2. The third ('Side Arm') flow path (Fig. 2A-3; 2B-3) was used for simultaneous attachment of up to six 47 mm filter holders or smaller absorbers. We used two for separate quantification of >0.4μm Si and for >0.4μm Ba and Mn (Poretics Polycarbonate, 0.4 μm, Osmonics, Inc.); About 30% of the time all side arm filter holders had a common 0.4 μm filter and the volume was apportioned by number of samples collected. When different filters/adsorbers were used we estimated flow through each type apportioned by flows measured under suction aboard ship.

Blank samples (filters mounted on a non-operating pump and lowered to depth for the cast duration) were processed identically to all other samples.

Aboard ship, MULVFS samples were photographed under controlled lighting using a NIKON COOLPIX 5700 digital camera (Lam and Bishop, 2007) and processed in depth order within 2 hours of the end of cast. All work was performed in a class 100 laminar-flow bench; non-contaminating gloves, sub sampling templates, scalpels, and tweezers were used. QMA filters were sub sampled for up to six other investigators using sharpened acid leached ~45 mm diameter acrylic tubes; "pie slice" sub samples equivalent to 1/8 to 1/4 of each >51 μm sample were cut using a stainless steel scalpel. When rare, larger zooplankton and small fish were removed from the MULVFS prefilter samples prior to sub sampling. The remaining sample was lightly 'misted' with 15 mL of 18.2 MOhm Milli-Q water under weak suction (<10 cm Hg) to reduce salt loading, oven dried at 60°C for 1-2 days, and then stored flat in trace metal certified polyethylene bags.

The "Side Arm" 0.4 μm filter samples were misted under mild vacuum with ~1.5 mL of Milli-Q water, and then transferred directly to acid leached 125 mL polyethylene bottles in which they were later analyzed. This eliminates fractionation of major sea salt components (e.g., Na from Ca).

Sample processing at Lawrence Berkeley National Laboratory was performed in a class-100 laminar flow fume hood in a class-10000 laboratory environment and followed Bishop et al., (1977, 1985). For analysis by Inductively Coupled Plasma Mass Spectrometer (ICP-MS), ~1/50th of each QMA filter was sub sampled following Bishop et al. (1985) and ~1/40th of each 51 μm prefilter was cut using a stainless steel scalpel (guided by eye to avoid zooplankton) using a rectangular acrylic template with recessed center. Sub samples were transferred to separate 125 mL acid leached – dried Nalgene® polyethylene bottles, flooded with 10 mL of 0.6 N ultra pure HCl (Seastar Chemicals Baseline Acid), and heated at 60°C overnight (~16 hours). Each leach solution was filtered (0.4 μm) and then diluted with 18.2 MOhm Milli-Q water to 50 grams weight. Solutions were further diluted (1:4) with Milli-Q water and treated with an indium spike (final In conc ~0.7 ppb) and then analyzed using a Finnigan Element II ICP-MS. Mixed element standards, and CASS III seawater, were prepared at multiple dilutions in the same 0.12 N HCl matrix. Elements determined were Li*, Na, Mg*, Al, P, K*, Ca*, Cr, Mn, Fe, Co, Ni, Cu, Zn, Rb, Sr*, Y, Cd, I, Cs, Ba, Tl, Pb, Bi, Ce, Nd, U*. Elements marked with asterisks (*) were corrected for sea salt components using Na (Bishop et al., 1977). Ca*, P, C_{org}, N, Sr*, Ba, and Mn are described in this paper. C_{org}, P, Ca*, and Si are listed in Tables 1 and 2. Other data are available from the author and public data archives

at Woods Hole Oceanographic Institution.

Groups from Woods Hole Oceanographic Institution (WHOI) and University of Tasmania (UTAS) were provided fresh filter sub samples for ^{234}Th, C and N, and for C_{org}, N, $\delta^{13}C_{org}$, and $\delta^{15}N$, respectively. The >51 μm material was rinsed from the polyester "pie slices" using 0.8 μm filtered seawater onto 25 mm diameter 0.4 μm silver filters, dried at 50 °C, and analyzed as described by Trull et al. (2008). A drying oven mishap resulted in loss of many of the QMA C_{org} samples from Cast M03 at ALOHA. The ^{234}Th samples were air-dried after/during counting aboard ship and stored frozen in Petri dishes for later analysis for C and N at WHOI. QMA in-situ sample blanks (~3 mg C per 25.4 cm diameter filter) were applied to the data. The use of in-situ blanks compensates for adsorption of dissolved species onto filters during filtration (Turnewitsch et al., 2007).

WHOI C_{org} and N data for QMA samples from cast M07 and M08 were low by factors of two to three compared with UTAS results (Tables 1 and 2). The M08 sub samples analyzed at WHOI had sat wet for considerable time before CN analysis (John Andrews, notes) and the same problem must have impacted their M07 sub samples. Similar problems may have affected some ALOHA samples from Cast M04, which also were not oven dried. We report all data but use the WHOI C_{org} QMA data for ALOHA (M1, M2, M4, M5) and the UTAS (combined <1 and 1-51 μm results) QMA C_{org} and N data for K2; The <1 μm WHOI results were retained for casts M07, 09, and 10 for comparison purposes. All >51 μm C_{org} samples at K2 and ALOHA were UTAS processed.

2.2 CTD Optics.

A WET Labs, Inc. (Philomath, OR) 25 cm path-length C-Star transmissometer (660 nm, receiver acceptance angle (RAA) of 1.5°) was interfaced to the SeaBird SBE 911 CTD (Bellevue, WA) and mounted horizontally at the bottom of the CTD/rosette frame. It was rotated in a way such that water would pass uninhibited through its beam as the CTD was lowered. This transmissometer was compared with a WET Labs C-Rover transmissometer (660 nm, 0.92° RAA), which was deployed during some MULVFS casts interfaced to a SeaBird SBE 19-plus data logger. Seapoint Sensors, Inc. (Exeter, NH) turbidity sensors (880 nm, scattering angle range 45 to 135 degrees, gain 100X) were also deployed during all CTD-rosette and MULVFS casts.

Accurate calculation of particle beam attenuation coefficient, C_P, requires compensation for analog to digital conversion electronics being used to read the sensor, compensation for sensor drift, and elimination of optics contamination while the sensor is not in the water. Briefly, on-CTD 'air' and 'zero' calibration of the transmissometer showed a ~1% loss of 'in air' transmission and zero offset due to the low impedence digitizing electronics of the Seabird 911 CTD. Pre- and post-cruise on-CTD and laboratory calibrations showed a transmission loss of 0.76% over 56 hours of profiling (103 CTD casts) at ALOHA and a 0.29% transmission loss over 95 hours and 86 casts in the colder waters of K2. Distilled water rinses of C-Star windows and their protection by plastic bottle caps between CTD casts eliminated optics contamination and the problem of cast offsets. The "cap" protocol was intermittently followed during the 2004 VERTIGO

ALOHA study and we had to resort to deep water matching methods (Gardner et al., 2006) for about 20-30% of profiles. This protocol was followed throughout the 2005 VERTIGO K2 study and no C_P data corrections were needed. Data dropouts occurred during ALOHA CTD casts 4 to 17 and during casts 39, 42, 43, 44, and 45. Few problems were encountered in K2 data.

Transmissometer profiles frequently showed sharp transient spikes to high C_P (e.g. Fig. 13 in Bishop et al., 1999) due to the transient blockage of the 25 cm by ~6 mm diameter transmissometer beam by zooplankton / larger phytoplankton and/or aggregate particles. For VERTIGO, the contrast between profiles from ALOHA and K2 was so striking (Fig. 3), that the data were processed to quantitatively track both spikes and continuum background (Appendix 1).

Spike C_P and scattering anomaly and spike abundance profiles were calculated using 20 decibar averaged down cast data pooled over 37 casts at ALOHA (D1 and D2 combined) and over 22 and 20 casts for K2-D1 and K2-D2, respectively. The spike abundance data were scaled by CTD lowering speed (range 40 to ~100 cm s^{-1}) using the assumption that each CTD scan (at 24 Hz) 'saw' a 1 cm layer of water. The C-Star beam volume is ~12 mL and the volume 'seen' by the Seapoint scattering sensor is approximately an order of magnitude smaller. Pooling C-Star results over 20 m for a single cast yields spike abundance statistics for a volume of ~ 25L; pooling 20 casts represents ~500 L. Similarly pooled scattering data builds abundance statistics for ~50L of seawater.

3. Results and Discussion

3.1 Dynamics of shallow waters at ALOHA and K2

Buesseler et al. (2008) described the hydrography and current regimes of the ALOHA and K2 sites. We summarize the variability of surface forcing (winds, short wave solar irradiance) and dynamic response of mixed layer temperature and mixed layer depth at K2 (Fig. 4) because these factors fluctuated more there than at ALOHA and because this variability is relevant to the understanding of major particle shifts observed at K2 described below.

The 24 hour mixed layer depth ($MLD_{0.05}$; depth of 0.05 potential density increase from a 5 m reference; Bishop et al., 2004) was 40 ± 10 m , and 14 ± 5 m (range 6 to 23 m) at ALOHA and K2, respectively. The deeper mixed layer at ALOHA reflected near steady trade wind conditions (~9 m s^{-1} winds). At K2, $MLD_{0.05}$ fluctuated strongly with forcing (Fig. 4). $MLD_{0.05}$ was at 10 m on day 207, but >15 m s^{-1} winds during days 209 and 210 increased $MLD_{0.05}$ to 23 m by the start if intensive studies. Winds during D1 and D2 (days 211-218 and 221-228) averaged 6.7 ± 1.9 and 6.2 ± 2.7 m sec^{-1}, respectively. Conditions during MULVFS casts were typical of D1 and D2 with the exception of M09, when winds averaged ~10 m s^{-1}. Nearly calm and foggy conditions (winds <4 m sec^{-1}) prevailed on day 215 and on days 224 through 227 when $MLD_{0.05}$ was shallower than 10 m. Sea surface temperature (SST) increased by ~0.1 °C d^{-1} indicating positive thermally

driven stratification. The low winds and stratification trend explains the very shallow mixed layer depths at K2.

Comparison of daily QUIKSCAT wind climatology at K2 showed that VERTIGO took place during the least windy 30 day period of the year and that the conditions VERTIGO sampled were typical (QUIKSCAT average for days 211-228 during 2002 and 2003 = 5.7 ± 3 m sec^{-1}). We note that late in the occupation of K2 (day 229) winds exceeded 20 m sec^{-1} and $MLD_{0.05}$ rapidly deepened to exceed 35 m; this event that may have triggered a secondary bloom seen after our departure by Honda (personal communication).

Boyd et al. (2008) reported rates of integrated primary production during VERTIGO to be 15.0±1.1 (ALOHA-D1), 18.3±1.7 (ALOHA-D2), 43±6.4 (K2-D1), and 31.4±5.7 mmol C m^{-2} d^{-1} (K2-D2). Euphotic depths were 125 m and 60 m for the two sites, respectively and the fraction of primary production occurring below the mixed layer was ~50% as ALOHA and ~60% at K2. The low productivity at ALOHA is consistent with nitrogen limitation of most of the euphotic zone (Karl et al., 1996; Casciotti et al., 2008). At K2, the declining productivity appears to be a response to quiescent conditions encountered. Iron limited conditions were found at 10 m, but not in deeper samples at K2 (Boyd et al., 2008).

The water column at ALOHA was primarily thermally stratified with mixed layer temperature exceeding 25 °C; K2 was both temperature and salinity stratified with mixed layer temperatures between 9 and 12 °C (Fig. 4 and 5). At K2, a temperature minimum

layer with waters colder than 2 °C was found between 80 and 150 m. This layer was relatively depleted of zooplankton (Steinberg et al., 2008; Fig. 6) and its signature was readily seen in particle fields observed with optics and directly sampled by MULVFS.

3.2 POC, zooplankton and in-situ pumps.

During VERTIGO we investigated the still troubling methodological question regarding particulate organic carbon (POC) observations, the contribution of zooplankton to POC, and whether zooplankton avoidance of in-situ pumps can explain differences in POC sampled by bottle and in-situ pumps (Liu et al. 2005). We compared MULVFS collections with a known efficient zooplankton sampler, the multi-depth IONESS (Intelligent Operative Net Sampling System; 1 m^2 net opening and 333 μm mesh; Kobari et al., 2008; Steinberg et al., 2008).

Briefly, Liu et al. (2005) discovered factors of 2-4 greater amounts of >0.7 μm POC in samples from wire deployed Niskin bottles vs. those from Challenger Oceanic in-situ pumps from the upper 50 m at the DYFAMED site (43°25.30'N, 7°53.52'E) in the Mediterranean Sea, but not in deeper samples. Samples collected at 20 m revealed ~40 fold differences in >70 μm POC and 20, 15, and 50 fold differences in radiolaria, copepods and copepod nauplii. Liu et al. (2005) hypothesized that the low POC levels were due to the efficient avoidance of pumps by zooplankton.

Photographic images of MULVFS >51 μm samples (resolved to ~50 μm) were analyzed

to determine abundances (# m^{-3}) of >1 mm zooplankton at K2 (Fig. 6). Copepod abundances at 10 m during casts M07, M08, M09, and M10 were 46 (day), 123 (night), 56 (day) and 153 (night), respectively. Chaetognath abundances at 10 m for the same casts were 0 (day), 2.6 (night), 0 (day), and 3.0 (night), respectively. Chaetognaths and copepods were rare in MULVFS samples in the temperature minimum zone (80-150 m; Fig. 6) and showed diurnal abundances changes at 235 m 0. (day) and 1.2 m^{-3} (night). Gelatinous siphonophores peaked in the 235 and 310 m samples at ~3 and 5 m^{-3}, respectively. Phaeodarian radiolarians peaked at 310 m with abundances ~5 (D1) and ~10 m^{-3} (D2), and were entirely absent from the upper 100 m.

Copepod abundances in day/night MULVFS casts at 10 m were consistently ~18% of the 0-50 m day/night IONESS abundances. Only several percent of IONESS copepods were trapped in deeper samples. Cast M09, taken in higher winds and seas, sampled fewest copepods throughout the water column except in the mixed layer suggesting that zooplankton below the mixed layer (and wave base) were able to easily detect and avoid pumps as they are being moved up and down by ship motion. We reproduced the systematic variation of chaetognaths with depth during casts M07, M08, M09, and M10 (0-50 m and 150-300m maxima) reported by Steinberg et al. (2008) but our numbers were ~10% of those reported.

In contrast, abundance profiles of siphonophores and radiolarians in MULVFS samples closely matched the IONESS data and, thus we conclude that slow- or non-swimming zooplankton such as siphonphores and radiolarians cannot avoid MULVFS. We found

that active swimmers such as copepods and chaetognaths were very successful at avoiding capture by pumps except in the turbulent surface mixed layer. Our greater capture of copepods in our mixed layer samples is consistent with Gilbert and Buskey (2005), who demonstrated that copepods are less able to detect suction currents (e.g. the opening mouth or feeding currents of predators) in the presence of turbulence.

There are multiple difficulties with the Liu et al. (2005) hypothesis. First, non-swimming radiolarians were 20-fold reduced in their in-situ pump samples, which we do not replicate. Second, the obvious differences they saw occurred in the shallow part of the water column, contrary to our finding of less pump avoidance by zooplankton in the mixed layer. Thirdly, the >70 μm POC levels reported by Liu et al. (2005) at 20 m were ~0.015 to 0.02 μM, and are significantly lower than we found at ALOHA (>51 μm POC 0.18 to 0.28 μM; Table 1), a location that is far more oligotrophic than the site they described. The only explanation of Liu et al. (2005) results is that they were an artifact of loss of most of the shallow >70 μm in-situ pump samples prior to recovery. We also cannot rule out artifacts due to inadequate sample preservation.

3.3 Particulate Organic Carbon - C_P relationships at ALOHA and K2.

C_P values have been used to estimate particulate organic carbon (e.g. Gardner et al. 1993, Bishop, 1999; Bishop et al. 1999, 2004; Gardner et al. 2006). Bishop et al. (1999) reported a consistent 16.1μM m^{-1} slope (and zero intercept) for C_P determined using a 1 m path length Sea Tech transmissometer (660 nm, 0.5° receiver acceptance angle, RAA)

and MULVFS POC. Bishop et al. (2004) reported a 30% loss of C_P sensitivity for a ~1.5° RAA prototype C-Rover (used on early Carbon Explorers) compared to the Sea-Tech 0.5° RAA instrument. During VERTIGO K2 we deployed a 0.92° RAA C-Rover transmissometer and found 18% enhancement of C_P relative to the C-Star (Fig. 7); comparison of the same 2 instruments in waters of the San Clemente Basin near San Diego, CA (June 2006) at higher particle loadings yielded a 22% higher sensitivity for the 0.92° RAA instrument, confirming the general loss of C_P response with wider receiver acceptance angle. The greater detection of forward scattered light by wider RAA instruments explains these differences. VERTIGO was the first time that C-Star C_P and MULVFS POC results have been directly compared.

The POC_{Cp} profiles at both ALOHA and K2 agreed well with MULVFS total POC (sum of <1, 1-51, and >51 μm C_{org}) using a conversion factor of 27 μM m^{-1} (Fig. 8A and B). As noted above, zooplankton had contaminated nighttime samples at 10 (and 230 m) at K2. If we use 0-50 m day and night zooplankton dry weight estimates (Steinberg et al., 2008), a ratio of 1.88 dry weight to C_{org} (Hedges et al. 2002), and our observed 18% copepod capture efficiency, then we calculate zooplankton carbon added ~0.2 and 0.9 μM C to the 10 m K2 samples day and night, respectively. Subtracting these bring the discrepant 10 m K2 POC data closer in line with POC_{Cp}. At ALOHA, zooplankton would account for ~0.05 ± 0.02 μM C above 50 m.

$$POC_{Cp} \text{ (K2 and ALOHA)} = 27 \bullet Cp \ \mu M\ C \qquad (1)$$

Figures 8C and 8D compare profiles of POC vs. POC_{scat} (turbidity scaled to deep water POC) at ALOHA and K2. POC_{scat} strongly underestimates POC in the euphotic zone at both ALOHA and K2.

3.4 Particle Optics at ALOHA and K2

3.4.1 Time series of POC_{Cp} and Turbidity

Figure 9 shows time series of POC_{Cp}, mixed layer depth ($MLD_{0.05}$), and distance from study area center at ALOHA and K2. At both sites, euphotic zone POC_{Cp} below the mixed layer was similar to or higher than mixed layer values with sharpest declines in concentration with depth corresponding to the base of the euphotic zone (125 m, ALOHA; 60 m, K2).

At ALOHA, mixed layer POC_{Cp} fluctuated diurnally with highest levels at dusk and lowest levels near dawn consistent net daytime production and nighttime grazing loss (Figure 10). Such variations are well recognized (Siegel et al., 1989; Gardner et al., 1993; Walsh et al., 1995; Bishop et al., 1999). Diurnal changes of ~0.3 μM relative to average concentrations of 1.2 μM imply a 4 day turnover time for POC in the mixed layer at ALOHA. Integration of dusk – dawn POC_{Cp} profile differences to 125 m and 200 m (Figure 8A) yield net primary production (NPP) values of 27 and 35 mmol C m^{-2}, respectively. Values agree with in-situ C-14 incubation results reported for ALOHA

(Karl et al. 1996), but are ~ 60% higher than the 16.6 mmol C m^{-2} d^{-1} NPP (125 m) results of Boyd et al. (2008) who used on-deck incubations during VERTIGO cruises.

At K2, POC_{Cp} decreased from between 4 and 5 μM (D1) to between 2 and 3 μM (D2) in the 60 m euphotic zone (Fig. 9). There was a progressive deepening of the particle maximum below the mixed layer with time from ~25-30 m (D1) to 40-45 m (D2). Buesseler et al. (2008) similarly noted a downward shift in the fluorescence maximum. Our data indicates that this shift paralleled that of biomass and thus was not a light adaptation response of the phytoplankton. Given that sub-mixed layer waters were stratified we calculate a phytoplankton sinking rate of ~1.5 m d^{-1} (15 m depth change over 10 days). The sinking may well be a reflection of the quiescent winds, and very shallow mixed layers at K2 during the VERTIGO study (Fig. 4). The 20-25% dusk / dawn profile differences for POC_{Cp} (Fig. 8B) indicate 4-5 day POC turnover times in the euphotic zone at K2. The 2-3 fold higher POC concentrations in the twilight zone at K2 vs. ALOHA reflect differences in POC fluxes reported by Buesseler et al. (2007).

Figure 11 shows that the time series for turbidity follows (but not proportionately) trends described for POC distributions (Fig. 9). At ALOHA, near constancy of particle abundance (save diurnal variations) was found in the euphotic layer. At K2, a greater than factor-of-two decrease in turbidity was observed in the upper 60 m between periods D1 and D2. K2 turbidity trends also indicated a temporal decline of particles contributing to light scattering within the 100-500 m depth interval. This decline is consistent with losses of Ca^{*} which are described in Sec. 3.5.2.

At both ALOHA and K2, the 'statistical funnel' of particle sources sampled by the sediment traps deployed at depths of 150 to 500 m was smaller than 40 km (Buesseler et al., 2008). For this reason, all CTD casts located within a distance of 30 km from central reference points, 22.75°N 158°W (ALOHA) and 47°N 161°E (K2), were analyzed to quantify the relative spatial and temporal variability of POC. We wish to understand if the large changes seen in POC_{Cp} and turbidity at K2 (Figs. 9 and 11) and in MULVFS data (Section 3.5) primarily reflect (1) a 1-D vertical ecosystem/particle field evolving over time or (2) different water columns sampled during the two intensive study periods. If we blank out data from farther than 30 km, the trends observed at K2 are most consistent with the interpretation (1). The lack of significant change of zooplankton biomass profiles (Steinberg et al., 2008) between D1 and D2 further reinforces this interpretation.

3.4.2 C_P and turbidity spikes: zooplankton or particles?

Are the transient spikes seen in transmissometer and scattering sensor profiles caused by large particles or zooplankton? Figure 12A quantitatively represents the contribution of transient spikes to C_P and turbidity profiles at ALOHA (D1 and D2 combined, 37 casts) and K2 time series (D1 22 casts; D2 20 casts). Figure 12B depicts spike abundance profiles for the same 20 m averaged/pooled data using spike duration as a crude indicator of particle size. We show profiles for all spikes lasting greater than 0.1 s (the time constant of the transmissometer) and from those lasting longer than 0.3 s. C_P spike

abundances represent ~1000 and 500 L at ALOHA, and both K2 periods, respectively; turbidity spikes, 10-fold less water.

At ALOHA, spike C_P and turbidity anomaly decreased strongly with depth (Fig. 12A) and accounted for ~1.2% of C_P (Fig. 3), and ~10% of turbidity at 30 m. Few C_P spikes were found below 200 m. At K2, C_P and turbidity spike anomaly at 30 m represented ~15% and ~10% of background values, respectively. In deeper waters, spike C_P anomaly showed a strong minimum in the temperature minimum zone (from 80 to 140 m), rose to a secondary maximum at ~270 m and then decreased to 1000 m. This pattern almost perfectly follows the double peaked distribution of zooplankton biomass described Steinberg et al. (2008). Spike C_P anomaly was one to two orders of magnitude stronger in the deepest twilight zone at K2 than at ALOHA.

At K2, abundances of >0.1 and >0.3 second spikes pooled from 20 to 40 m were ~1600 and 700 m^{-3} (D1) and 800 and 300 m^{-3} (D2), respectively. Abundances were almost invariant near the 270 m maximum (~ 400 m^{-3} and ~100 m^{-3}, respectively) for both D1 and D2. The 0.3 s transmissometer spike abundance profiles are very comparable to the IONESS zooplankton abundance profiles, especially in sub-euphotic zone waters. The fact that both 0.1 and 0.3 abundance profiles 'look' like zooplankton biomass trends and did not change with time at 270 m suggests that they are due to living organisms. The C_P spike profile is thus best explained by transient encounters of zooplankton with the transmissometer beam at 40-100 cm s^{-1} CTD lowering speeds.

Turbidity spike abundance profiles at ALOHA and K2 showed a 20 times greater frequency of occurrence and differing profile shapes than seen in transmissometer data. For example, at K2 the there was no minimum in the temperature minimum layer, and at ALOHA, the 0.1 s spike profile had a secondary maximum in the deep chlorophyll maximum. The profile trends at K2 are very reminiscent of changes seen on Ca^* and Si distributions (described below). Thus, it is likely that the scattering spike trends are a direct reflection of abundances of larger or chained phytoplankton and possibly aggregate particles in the water column. The fact that the active sampling volume of the scattering sensor is 1-2 cm from the sensor explains why there is little zooplankton signal and why more numerous, but smaller particles would dominate in its record. C_P and scattering spikes rarely co-occurred at the same time (or appropriately lagged in time), indicating their different origins. We thus reject the hypothesis that aggregate particles contribute to the majority of the spikes in transmissometer records. No chemical (Section 3.5) or photographic metric (Lam and Bishop, 2007) of aggregate abundance on MULVFS prefilters showed a minimum in the temperature minimum zone and maximum near 300 m. We note however, that spike abundance profiles from the turbidity sensor appear to be more comparable to records derived from marine snow cameras (e.g. Lampitt et al., 1983). This may be explained by the fact that turbidity sensors and marine snow cameras derive their signals/images using reflected (and not transmitted) light. Particles must be significantly absorbing to be seen by transmissometers.

3.5 *Size-Fractionated Particulate Matter Chemistry and Budgets*

The >51μm samples collected by MULVFS contain particles contributing mostly to sedimentation and the <51μm size fractions represent the slowly sinking material that in most cases dominates particulate matter concentration. Exceptions occur in the euphotic zone where >51 μm phytoplankton, protist grazers, and zooplankton (discussed above) can dominate particle concentrations. As we will show, the small slow-sinking particle fraction can be very dynamic since it is influenced on very short time scales by imbalances in the rates of particle addition due to aggregate fragmentation and particle losses as a result of aggregation; both are biologically mediated.

Concentration profiles of particulate C_{org}, N, P, Ca^*, Si, Sr^*, Ba, and Mn from MULVFS show major differences between the oligotrophic waters of ALOHA and the more productive waters at K2 (Figs. 13 to 16). In all cases, a reference to these elements in the text implies their occurrence in particulate form. We interchangeably refer to C_{org} as POC, and Ca^* as PIC or C_{inorg}. In the figures, one trend line will be drawn for the average of all ALOHA data (M01 through M04) consistent with the finding of small changes in most biological parameters (Buesseler et al., 2008) and optics data presented above. At K2, large changes in particulate pools and size fractionation occurred over the 10 days separating our paired MULVFS casts; thus averages for K2-D1 and K2-D2 are denoted by separate lines. Open and closed symbols identify daytime and nighttime casts, respectively.

3.5.1 Particulate C_{org}, N, and P

Figure 14 shows that C_{org} and P in all of the "<1", 1-51, and >51 μm MULVFS size fractions are lower at ALOHA than at K2 through out the twilight zone to 900m. The only exception to this rule was the 60-150 m depth interval, which included the euphotic zone at ALOHA but was below euphotic layer at K2 (Boyd et al., 2008).

The >51 μm C_{org} sub samples included zooplankton trapped by MULVFS and their contribution to the profiles is readily evident in the diurnal concentration differences at K2 (Fig. 13), particularly at 10 m (night high by a factor of 2.5), 235 m (night high by 3.5), and 310 m (night low by 2). The higher nighttime C_{org} at 235 m is explained by more zooplankton, particularly chaetognaths, being captured by MULVFS in the darkness than during the day (Sec 3.2). During K2-D1, >51 μm C_{org} (Fig. 13) decreased twelve-fold with depth from 0.50 μM at the base of the euphotic layer (60 m) from to ~0.04 μM at 500 m; ten days later (D2) >51 μm C_{org} decreased two-fold from ~0.10 μM to ~0.05 μM over the same depth interval. At ALOHA, >51 μm C_{org} decreased five-fold from 0.085 μM near the base of the euphotic layer (125 m) to 0.017 μM at 570 m.

At K2, >51 μm C_{org} accounted for 30 and 15% of total C_{org} in the non-zooplankton influenced samples at 35 m during D1 and D2, respectively. Similarly, >51 μm C_{org} was ~16% of total C_{org} at ALOHA. At 150 m, 300 m, and 500 m depths corresponding to NBST observations, >51 μm C_{org} comprised 16%, 15%, and 10%, respectively during K2-D1; 8%, 16%, and 15% (K2-D2); and 16%, 10% and 12% at ALOHA. The reversal of percentages with depth between K2-D1 and K2-D2 is also reflective of the strong transient decrease of carbon sedimentation at K2 reported by Buesseler et al. (2007).

During K2-D1, <51 μm C_{org}/N (combined <1 and 1-51 μm fractions) varied from 5.5 to 6.0 in the upper 100 m and from 6 to 7 in deeper waters (Fig. 14). Values shifted slightly lower (between 6 and 6.5) in the 150-500 m interval during K2-D2. During K2-D1, >51 μm C_{org}/N increased from ~6 at 35 m to ~9 at 85 m in the temperature minimum layer, decreased to ~6 at 235 and 300 m and increased to ~7.5 by 800 m. D2 trends were similar, except in the euphotic zone samples. The minimum at 235 and 300 m reflects the secondary peak in zooplankton biomass (Steinberg, et al., 2008).

At ALOHA, <51 μm C_{org}/N decreased from 7.8 in the upper 50 m to ~6 at the depth of the deep chlorophyll maximum (DCM) ~125 m, and increased to 8 below 300 m. >51 μm C_{org}/N decreased from ~8 in the mixed layer at 30 m to ~5 in the DCM near 100 m, followed by a gentle increase to 6 by 500 m. The C_{org}/N trends are consistent with prior observations of the upper water column at ALOHA (http://hahana.soest.hawaii.edu/hot). There was little evidence of significant changes over time between the two pairs of MULVFS casts. The surface to DCM C_{org}/N shift reflects a change from a shallow nitrogen fixation dominated system to one supported by dissolved nitrate (Karl et al., 1995; Casciotti et al., 2008).

Phosphorus profiles (Fig. 13) generally followed C_{org} trends described above for all size fractions but were better behaved than for C_{org}. This primarily reflects the fact that phosphorus is not lost from samples due to lack of drying and that our >51 μm sub sampling scheme tried to avoid contaminating zooplankton. The >51μm P at K2

exceeded ALOHA values by a factor of ten both in surface waters and below 500 m, reflecting grossly the order of magnitude differences in flux reported for these two locations (Buesseler et al., 2007).

At K2, >51 μm P decreased and both <1 and 1-51 μm P increased in the 105 to 350 m interval between D1 and D2, suggesting a net increase in the fragmentation rate of large sinking particles (and increased bacterial activity at depth) had enriched the subsurface small particle pool in labile organic material over the time of our observations.

>51 μm P decreased more strongly than C_{org} through the twilight zone indicating preferential remineralization of P from the large size fraction during sinking, consistent with the labile behavior of phosphorus relative to carbon (e.g. Collier and Edmond, 1984). During K2-D1, >51 μm C_{org}/P ratio increased with depth from ~91 at 35 m to ~175 in deeper samples (zooplankton contaminated samples at 235 m with C_{org}/P = 450 and 680 ignored). During K2-D2, >51 μm C_{org}/P was ~150 at depths from base of the euphotic layer to 310 m and increased to ~300 in deeper waters.

At ALOHA, >51 μm C_{org}/P increased with depth from ~120 at 30 m to ~300 by 500 m. Deeper data are not available. The lower >51 μm C_{org}/P with depth during K2-D1 reflects faster transfer of both carbon and phosphorus (Buesseler et al., 2007). The more degraded signature of the >51 μm particles during K2-D2 is also consistent with the findings of Trull et al. (2008) who found a significant decrease in particle selling velocity between D1 and D2.

Our C_{org}/P profiles at both locations are in agreement with longer remineralization lengths for C_{org} vs. P inferred from sediment trap samples (Lamborg, et al., 2008).

3.5.2 Particulate Inorganic Carbon and Opal.

Ca^* (Ca in samples corrected for sea salt Ca) is a close measure of particulate inorganic carbon (PIC, C_{inorg}; Bishop et al. 1977), which can range in surface ocean waters between 10's of nM and 40 μM (in coccolithophores blooms). Ca^* in 1-51μm and >51μm fractions (Fig. 15) at both K2 and ALOHA were at the lower end of the oceanic range. Concentrations of <1 μm Ca^* were negligible at all depths, indicating that micron sized coccoliths were predominantly retained by the first (1-51 μm) QMA filter.

At ALOHA, 1-51 μm Ca^* varied between 15 and 65 nM in the 125 m deep euphotic zone with highest levels near the deep chlorophyll maximum (DCM). Our results are consistent with prior descriptions of coccolithophore abundance profiles at ALOHA (Cortes et al., 2001). 1-51 μm Ca^* below 200 m ranged between 20 and 30 nM and there was no obvious change over time. >51 μm Ca^* decreased from ~8 nM at the base of the euphotic layer to between 1 and 2 nM at 800 m.

At K2, Ca^* (PIC) varied strongly in both large and small particle size fractions between the two study periods (D1 and D2). Highest 1-51 μm Ca^* (55-90 nM) was found at 35 m during D1. Ten days later, Ca^* had dropped to <10 nM at the same depth. Four-fold losses were seen in >51 μm Ca^* at 35 m over the same period. Scanning electron

microscopic (SEM) imaging of our samples confirmed coccolithophores in the 1-51 μm fraction, especially during K2-D1.

At ALOHA, 1-51 μm C_{org}/C_{inorg} was approximately 30 in the mixed layer, ~10 at 155 m, and decreased to ~3 at 500 m. >51 μm C_{org}/C_{inorg} depth trends were identical. At 35 m at K2, 1-51 μm C_{org}/C_{inorg} increased ten fold over 10 days from ~26 (D1) to 240 (D2); at the same time the >51 μm fraction increased modestly from 16 to 25. Factor of two or more shifts of C_{org}/C_{inorg} in the 1-51 μm (23 to 50) and >51 μm fractions (13 to 35) in sub euphotic layer samples further attest to the rapid changes of particle pools in the twilight zone at K2.

Biogenic Si determined in >0.4 μm "Side Arm" samples (Fig. 2; Fig. 15) was ~100 times higher (3μM) in K2 surface waters compared with ALOHA (~20 nM), consistent with the strong silica enhancement of sedimentation fluxes at K2 (Honda et al. 2002). Our ALOHA Si data are comparable to values for 'non-bloom' waters of the central Pacific Gyre to the north of ALOHA at 26 and 29 °N (Brzezinski et al., 1998). Particulate Si observations have not been reported at K2.

At K2, >51 μm Si in the euphotic layer dropped by a factor of 6 over the ten-day interval between D1 and D2. The drop paralleled closely changes in the abundance of turbidity spikes detected by the turbidity sensor (Fig. 12) and suggests that many of the turbidity spikes were due to larger individual and chain forming diatoms. The fraction of total Si in the >51 μm size fraction dropped from ~60% to ~30% over the same period, paralleling

changes in $\%C_{org}$ described above and the size fractionated productivity results of Boyd et al. (2008).

3.5.3 Particulate Sr, Ba, and Mn.

Particulate strontium (Fig. 16) occurs at very high concentrations when $SrSO_4$ forming Acantharia are present (Bishop et al., 1978); furthermore, Acantharia growth, sedimentation, and shallow dissolution is believed to be the major factor explaining the 1-2% depletion of Sr/Cl ratio in surface waters of the Pacific (Bernstein et al., 1987). At ALOHA, >51 μm Sr^* was unusually elevated (4 nM) in the surface mixed layer. The 3 orders of magnitude decrease of >51μm Sr^* with depth to 800 m is consistent with strong dissolution and mechanical fragmentation of Acantharia structures during sedimentation (Bishop et al., 1977). At ALOHA, the factor of five >51 μm Sr^* decrease between 150 and 500 m exactly matches the decrease of Sr flux in NBST samples at these depths (Lamborg et al., 2008). At K2, >51 μm Sr^* peaked below the euphotic layer at 200-300 pM (D1) near 100 m. Much of the Sr^* is present either as a minor component of carbonates or absorbed by abundant Mn and Fe oxides (Lam and Bishop, 2008).

Barium (Figure 16) has been linked to carbon export (Dehairs et al. 1980, Bishop 1988). The most notable feature in the comparison of ALOHA and K2 was the shallow intense double subsurface maximum of 1-51 μm Ba (300 – 600 pM) at K2 between 85 and 250 m. High levels of >51 μm Ba (between 80 and 100 pM) occurred during K2-D1 at the same depths consistent with barite formation in the >51 μm fraction and shallow breakup

the large aggregates being the source for the smaller particles. Buesseler et al. (2007) found particulate C_{org} fluxes at K2 to be initially 10 times more elevated than at ALOHA. The >51μm Ba parallels this trend exactly (Fig. 16) confirming the link to sedimentation. Dehairs et al. (2008) discuss the relationship of stocks of Ba in subsurface waters to bacterial activity of the same waters. The link of enhanced subsurface metabolism and concentrations of <51 μm Ba is consistent with the Ba-export connection.

Manganese (Fig. 16) in the 1-51μm fraction at K2 displays a classic signature of material rapidly delivered from the continental margin sediment sources at a depth of 135 m (Lam and Bishop, 2008). In contrast to biogenic elements, Mn has little supply from surface waters and thus readily reflects lateral supply processes at depth. We found that >51μm Mn exceeded 1-51μm Mn by a factor of 5 in the euphotic zone during K2-D1. It appears that organisms feeding on small particles near the 135 m Mn maximum are migrating vertically and producing Mn enriched large particles at shallower depths. This is an example of an alternate route by which reactive metals can be transported vertically to fuel biological processes in the euphotic zone.

3.5.4. Euphotic to Twilight Zone Budgets for $CaCO_3$ and opal, C_{org}, and Ba.

$CaCO_3$ production by coccolithophores at ALOHA and K2 was estimated from integrated 5-20 μm net primary productivity (NPP) data of Boyd et al. (2008) and the C_{org}/Ca^* ratio of the 1-51 μm fraction averaged over the euphotic layer. Some C_{org} is smaller than 5 μm and some of Ca^* is present as coccoliths; however, these errors are likely to cancel. At

ALOHA, 12.9 and 11.1 % of NPP was in the 5-20 μm fraction, C_{org}/Ca^* ratios were 34 and 31, and $CaCO_3$ production was thus estimated to be 0.057 and 0.065 mmol C_{inorg} m^{-2} d^{-1} for D1 and D2, respectively. At K2, $CaCO_3$ production was estimated to be 0.888 and 0.016 mmol C_{inorg} m^{-2} d^{-1}, using 10.8 and 12.2 % of NPP in the coccolithophore size fraction and C_{org}/Ca^* ratios of 63 and 246 for the D1 and D2 periods, respectively.

Biogenic Si production was similarly estimated using the Boyd et al. (2008) measurements of >5 μm NPP and C_{org}/Si ratios estimated for the >1 μm particulates, where C_{org} is summed for 1-51 μm and > 51 μm fractions and Si is > 0.4 μm Si (Tables 1 and 2). The ratio approach compensates for presence of <5 μm C_{org} and siliceous fragments in the samples. Where >51 μm C_{org} data was absent at ALOHA, this fraction was estimated using >51 μm P and the C_{org}/P ratio of the sample immediately shallower or deeper (Table 1). At ALOHA, 24 and 21 % of NPP was in the >5 μm fraction, C_{org}/Si was 43 and 53, and Si production was thus estimated to be 0.083 and 0.072 mmol Si m^{-2} d^{-1} for periods D1 and D2, respectively. At K2, 40 and 28 % of NPP was in the 'diatom' fraction, C_{org}/Si was 1.62 and 2.07, and Si production was estimated to be 10.7 and 4.3 mmol Si m^{-2} d^{-1} for K2-D1 and K2-D2, respectively. The Si/Ca^* production ratio was 1.45 and 1.1 at ALOHA and was 12.1 and 276 at K2 for periods D1 and D2, respectively.

While there was little of change in Ca^* standing stocks at ALOHA from D1 to D2, at K2 Ca^* in all particle size fractions declined sharply throughout the water column (to at least 700 m) over 10 days between D1 and D2 (Fig. 15). Integrated (800 m to the surface) standing stocks of 1-51 μm Ca^* (Fig. 17) decreased 40% over 10 days from 17.7 mmol

m^{-2} (D1) to 11.1 mmol m^{-2} (D2) implying a net Ca^* loss of 0.66 mmols m^{-2} d^{-1}. Similarly integrated >51 μm Ca^* stocks dropped three-fold from 7.6 mmol m^{-2} (D1) to 2.9 mmol m^{-2} (D2) over 10 days indicating a net PIC loss of 0.47 mmols m^{-2} d^{-1}. The total rate of loss of carbonate was 1.13 mmols m^{-2} d^{-1} with most lost occurring in waters shallower than 500 m. Carbonate particle stock changes exceeded the average rate of carbonate production at K2.

Figure 18 compares rates of Ca^* production (derived above) and Lamborg et al. (2008) NBST fluxes for both ALOHA and K2 waters. Our production estimates at K2 are close to observed NBST fluxes at ALOHA and there is little evidence for carbonate dissolution in the twilight zone. The apparent lack of PIC remineralization at ALOHA is consistent with the 400% calcite supersaturation of surface waters and the presence of the 100% saturation horizon at 700 m (Sabine et al., 1995).

At K2, there was abundant evidence for strong carbonate dissolution in the twilight zone (Fig. 19). The percentage of shallow carbonate dissolution (D_{CaCO3}) is:

$$D_{CaCO3} = (1 - (E_{500}/(P_{EZ} - \Delta S)))\bullet 100 \quad \% \qquad (2)$$

where, E_{500} is the average 500 m NBST flux for K2-D1 and K2-D2, P_{EZ} is average carbonate production (estimated above), and ΔS = the standing stock change for carbonates (D2 – D1). P_{EZ}, $E_{500,}$ and ΔS are ~0.45, ~0.13, -1.13 mmols m^{-2} d^{-1}, respectively at K2, yielding D_{CaCO3} = 92%, the percentage of carbonates produced and

present in the water column dissolved. Without consideration of stock changes, only 70% of the carbonate particles would be considered dissolved in the upper 500 m at K2. The transition from carbonate saturated to undersaturated waters occurs ~200 m at K2 and anomalies in dissolved carbonate system parameters reflect shallow and intense carbonate dissolution (Feely et al. 2002). Our observations at K2 show dissolution effects shallower than 200 m and dictate that the strong shallow carbonate removal must be a result of zooplankton enhancement of dissolution during particle capture and repackaging. Similar particle-based evidence for strong biologically mediated carbonate dissolution was found in the Panama Basin in the eastern equatorial Pacific, a location where the calcite saturation depth occured near 300 m and the water column was just under saturation to a depth of 1500 m (Bishop et al., 1986).

For Si at ALOHA, P_{EZ} ~0.08 mmol m^{-2} d^{-1}, integrated stocks changed little, and E_{500} was ~0.04 indicating D_{silica} ~50%. At K2, P_{EZ} was 7.5 mmol m^{-2} d^{-1}, E_{500} ~4 mmol Si m^{-2} d^{-1}, >51 μm Si stock change (Fig. 17) was -7.1 mmol Si m^{-2} d^{-1} and occurred in the upper 100 m, while the <51 μm fraction gained fragmented Si at a rate of 3.7 mmol Si m^{-2} d^{-1} giving a ΔS = -3.4 mmol Si m^{-2} d^{-1}. We estimate that approximately 65% of the Silica dissolved in the twilight zone at K2. These estimates are consistent with other biogenic Si production and dissolution observations summarized by Nelson et al. (1995) for the global ocean.

We could not estimate rates of barite precipitation in the water columns at either ALOHA or K2 because Ba is not linked with carbon during the primary production step. At K2,

column integrated stock changes (D1 to D2) for Ba to from 800 m to surface (Fig. 18) imply a loss from both 1-51 and >51 μm size fractions of 4.95 μmols Ba m^{-2} d^{-1}. This loss is 10 times greater than measured fluxes in NBSTs (~0.54 (D1) and 0.58 (D2) μmols Ba m^{-2} d^{-1}) reported by Lambourg et al. (2008) and implies that rapid shallow barite dissolution was occurring at K2.

POC remineralization efficiency at K2 and ALOHA can be contrasted with the above findings. At K2, P_{EZ} ~38, ΔS ~ -8 (from Fig 8 profiles), and E_{500} = 1.7 mmol Corg m^{-1} d^{-1} (Lamborg et al., 2008), implying a ~96% remineralization efficiency for primary produced carbon in the upper 500 m at K2. Similarly, P_{EZ} at ALOHA = 16.7, ΔS ~ 0, and E_{500} = 0.31 mmol Corg m^{-1} d^{-1} yields a 98% utilization of primary produced carbon.

4. Summary and Conclusions

The VERTIGO experiment offered comprehensive observations of the particle dynamics in the upper 1000 meters at oligotrophic station ALOHA and productive station K2 by many investigators. The combination of MULVFS sampling with comprehensive characterization of major and minor particulate matter phases (never before performed at either site), and CTD deployed transmissometer and scattering sensors provided unique observations of the vertical profiles and high-frequency variations of particulate matter and hence clear insight into the biological processes governing particle abundances, chemistry, and sedimentation in the twilight zone.

As part of the VERTIGO project, new protocols for treatment of transmissometer sensors routinely deployed on CTDs introduced at ALOHA and successfully implemented at K2, permitted accurate quantification of particle beam attenuation coefficient, eliminating the need for profile matching in deep water. The MULVFS POC C_P relationship (~27 μM m^{-1}) was established for the C-Star transmissometer and applied equally well to highly oligotrophic waters at ALOHA and productive waters of K2, despite large relative differences of C_{org}, C_{inorg}, and Si phases and their partitioning among different size fractions. Turbidity (from scattering) – POC relationships are poor by comparison.

We investigated how spikes in transmissometer and turbidity sensor records reflect the structure of the food web and ecosystem processes. Our results indicate that spikes in transmissometer profiles are due to zooplankton. Spikes do not reflect abundances of sinking particles in the water column. Those of the scattering sensor mostly appear to reflect abundances of larger and chain forming phytoplankton, protist grazers and possibly large aggregates. Nearly transparent particles like marine snow are not readily detected in transmitted light but are easily detected using reflected light.

We investigated the Gardner et al. (2003) and Liu et al. (2005) reports of major biases between POC measured in bottle samples and in-situ pumps. We documented sample preservation biases (two groups analyzing the same MULVFS sub-samples) that led to factor of three differences and present evidence that the in-situ pumps compared in both the Gardner et al. (2003) and Liu et al. (2005) studies had most likely failed to retain sample prior to recovery.

Analysis of time series data on variations of particle beam attenuation coefficient, C_P, and turbidity within 30 km (or the statistical funnel of particle sedimentation) of our study areas supported an interpretive framework that ecosystem processes from the mixed layer through the twilight zone operated on sufficient spatial scale (or were sufficiently spatially homogeneous) at both ALOHA and K2 that the water column could be treated as a 1D (depth) system evolving in time with respect to major biogenic particulate phases C_{org}, N, P, $CaCO_3$, Si, Sr, and Ba.

Turnover times of C_{org} in the euphotic layers at both K2 and ALOHA were of the order of 4 to 5 days. Similar time scales are inferred for all particle fractions in the twilight zone at K2 based on considerations of C_{org}/N, $CaCO_3$, and Si changes over time.

We demonstrated that mass balances for the twilight zone can be substantially affected by changes in large and small particulate pools. Substantial (92%) shallow carbonate dissolution was found in the twilight zone at K2; while minor evidence for dissolution was found at ALOHA, consistent with carbonate saturation chemistry at the two sites. Shallow carbonate dissolution at K2 could not have occurred without substantial biological enhancement of the process. ~50% and 66% of produced Si, dissolved in the twilight zones at ALOHA and K2, respectively. These results underscore the merit in simultaneous determination of particle concentration and flux profiles, especially in biologically dynamic regimes.

NBST and primary productivity data showed that the ecosystem at K2 allowed only a factor of two higher (4% vs. 2%) penetration of primary produced carbon to 500 m than found at ALOHA. At the same time, Buesseler et al. (2007) showed that the transfer efficiency (change of flux between two depths) of sinking particles between 150 m and 500 m was significantly higher at K2 than at ALOHA. The higher transfer efficiency is partially explained by the avoidance of the temperature minimum zone at K2 by most zooplankton, coupled with a strong harvesting of sinking particles (by zooplankton) in warmer waters just below the base of the euphotic zone. Such action also explains the strong observed gradients of particulate phosphorus and carbon between 60 and 150 m.

The action of the zooplankton community was strong and layered at K2 (Steinberg et al., 2008; Wilson et al., 2008; Kobari et al., 2008) and it is clear that sinking particles must pass through the gauntlet active particle feeders as they pass through the twilight zone to 1000 m. Distinctly layered zones of particle transformation (and the active role of migrating and non-migrating zooplankton as agents of particle transformation) has been long recognized (Karl and Knauer, 1984; Bishop et al, 1986; Angel, 1989). Signatures of transformation are readily seen in the sampled particulates and optics data. At K2, the likelihood that a particle can leave the euphotic layer and pass through the twilight zone without being intercepted and repackaged multiple times is small.

Clearly, VERTIGO sampled a highly transient regime at K2 in quiescent summertime conditions. Such intensive process level observations can begin to inform sophisticated ecosystem/particle flux simulations (e.g. Jackson and Burd, 2002) since they provide both

comprehensive views of the ecosystem and of particle abundances, chemistry, and flux. However, high frequency observations of biogenic particulate stocks and fluxes from surface through twilight zone on yearly time scales are needed to fully inform biogeochemical models (e.g. Dunne et al., 2005; Gehlen et al., 2006) and thus enable predictability of future changes to the substantial 10 Pg C y^{-1} flows through the ocean's biological pump.

Acknowledgements.

We thank masters and crews of R/V Kilo Moana and R/V Revelle for excellent support at sea. Captain D. Murline and his engineers and deck crew deserve special mention for effort far exceeding the expected in getting MULVFS aboard R/V Revelle and fully secured and operational in the early morning hours of the morning of departure from Yokohama. We thank many in the VERTIGO project who provided assistance during MULVFS casts and for helping make the CTD/optics program a success. Particularly, we thank K. Buesseler, chief scientist (WHOI); T. Trull (co-chief scientist) and colleagues (University of Tasmania), F. Dehairs, W. Behrens and M. Elskens (U Brussels); M. Gall (NIWA, New Zealand), and K. Casciotti (WHOI). We thank T. Trull, K. Buesseler, and M. Honda and anonymous reviewers for very thoughtful comments on this paper. Funding for our participation in VERTIGO was provided by the US Department of Energy, Office of Science, Biological and Environmental Research Program under Cont. No. DE-AC02-05CH11.

REFERENCES

Angel, M.V., 1989. Does mesopelagic biology affect the vertical flux? In: Berger, W.H., Smetacek, V.S., Wefer, G. (Eds.), Productivity of the ocean: Present and past. John Wiley and Sons Limited, New York, pp. 155-173.

Armstrong, R.A., Lee, C., Hedges, J.I., Honjo, S., Wakeham, S.G., 2002. A new, mechanistic model for organic carbon fluxes in the ocean based on the quantitative association of POC with ballast minerals. Deep-Sea Research II, 49(1-3), 219-236.

Bernstein, R.E., Betzer, P.R., Feely, R.A., Byrne, R.H., Lamb, M.F. and Michaels, A.F. (1987). Acantharian Fluxes and Strontium to Chlorinity Ratios in the North Pacific Ocean. Science 237, 1490-1494.

Bishop, J.K.B., Edmond, J.M., 1976. A new large volume filtration system for the sampling of oceanic particulate matter. Journal of Marine Research 34, 181-198.

Bishop, J.K.B., Edmond, J.M., Ketten, D.R., Bacon, M.P., Silker, W.B., 1977. The chemistry, biology, and vertical flux of particulate matter from the upper 400 m of the equatorial Atlantic Ocean. Deep-Sea Research 24, 511-548.

Bishop, J. K. B., Ketton, D. R., Edmond, J. M., 1978. The chemistry, biology and vertical flux of particulate matter from the upper 400 m of the Cape Basin in the southeast Atlantic Ocean. Deep-Sea Research, 25, 1121-1161.

Bishop, J.K.B., Schupack, D., Sherrell, R.M., Conte, M., 1985. A multiple unit large volume in situ filtration system (MULVFS) for sampling oceanic particulate matter in mesoscale environments. In: Zirino, A. (Ed.) Mapping Strategies in Chemical Oceanography, Advances in Chemistry Series, Vol. 209. American Chemical Society, Washington, DC, pp. 155-175.

Bishop, J.K.B., Stepien, J.C., Wiebe, P.H., 1986. Particulate matter distributions, chemistry and flux in the Panama Basin: response to environmental forcing. Progress in Oceanography 17 (12), 1-59.

Bishop J. K. B. and Fleisher, M. Q., 1987. Particulate manganese dynamics in the Gulf Stream warm-core rings and surrounding waters of the N.W. Atlantic. Geochim. Cosmochim. Acta 51, 2807- 2825.

Bishop, J.K.B., 1988. The barite opal organic carbon association in oceanic particulate matter. Nature 332 (6162), 341-343.

Bishop, J.K.B., Davis, R.E. and Sherman, J.T. (2002) Robotic Observations of Dust Storm Enhancement of Carbon Biomass in the North Pacific. Science 298, 817-821.

Bishop, J.K.B., Wood, T.J., Davis, R.E., Sherman, J.T., 2004. Robotic observations of enhanced carbon biomass and export at 55 degrees S during SOFeX. Science 304,

417-420.

Boyd, P.W., Gall, M.P., Silver, M.W., Bishop, J.K.B., 2008. Quantifying the surface-subsurface biogeochemical coupling during the VERTIGO ALOHA and K2 studies. *Deep-Sea Research II*.

Buesseler, K.O., Lamborg, C.H., Boyd, P.W., Lam, P.J., Trull, T.W., Bidigare, R.R., Bishop, J.K., Casciotti, K.L., Dehairs, F., Elskens, M., Honda, M., Karl, D.M., Siegel, D.A., Silver, M.W., Steinberg, D.K., Valdes, J., Van Mooy, B., Wilson, S.E., 2007. Revisiting carbon flux through the ocean's twilight zone. Science 316, 567-570.

Buesseler, K.O., Trull, T.W., Steinberg, D.K., Silver, M.W., Siegel, D.A., Saitoh, S.-I., Lamborg, C.H., Lam, P.J., Karl, D.M., Jiao, N.Z., Honda, M.C., Elskens, M., Dehairs, F., Brown, S.L., Boyd, P.W., Bishop, J.K.B., Bidigare, R.R., 2008. VERTIGO (VERtical Transport In the Global Ocean): a study of particle sources and flux attenuation in the North Pacific. Deep Sea Research Part II: Topical Studies in Oceanography.

Brzezinski, M.A., Villareal, T.A., and Lipschultz, F., 1998. Silica production and the contribution of diatoms to new and primary production in the central North Pacific. Mar. Ecol. Prog. Ser. 167, 89-104.

Broecker, W.S. and Peng, T.-H. (1982) *Tracers in the Sea*. Eldigio Press. 690 pp.

Casciotti, K.L., Glover, D., Trull, T., Davies, D., 2008. Constraints on Nitrogen Cycling at the Subtropical North Pacific Station ALOHA from Isotopic Measurements of Nitrate and Particulate Nitrogen. Deep-Sea Resarch II.

Charette, M.A., S.B. Moran and J.K.B. Bishop (1999) ^{234}Th as a tracer of particulate organic carbon export in the subarctic Northeast Pacific Ocean. Deep-Sea Research II 46(11-12) 2833-2862.

Collier, R.W. and Edmond, J.M., 1984. The trace element geochemistry of marine biogenic particulate matter. Progress in Oceanography, 13, 113-199.

Cortes, M.Y., Bollmann, J, Thierstein, H.R. (2001). Coccolithophore ecology at the HOT station ALOHA, Hawaii. *Deep-Sea Research II* 48, 1957-1981.

Dehairs, F., Chesselet, R., Jedwab, J., 1980. Discrete suspended particles of barite and the barium cycle in the open Ocean. Earth and Planetary Science Letters, 49, 528-550.

Dehairs, F., Jacquet, S., Savoye, N., Van Mooy, B.A.S., Buesseler, K., Bishop, J.K.B., Lamborg, C., Elskens, M., Baeyens, W., Boyd, P., Casciotti, K.L., Monnin, C., 2008, this volume. Barium in Twilight Zone suspended matter as a proxy for particulate organic carbon remineralization: Results for the North Pacific. *Deep-Sea Research II*.

Dunne, J. P., Armstrong, R. A., Gnanadesikan, A. and Sarmiento, J. L. (2005), Empirical

and mechanistic models for the particle export ratio. Global Biogeochem. Cycles 19, 4026, doi:10.1029/2004GB002390.

Feely, R.A., Sabine, C.L., Lee, K., Millero, F.J., Lamb, M.F., Greeley, D., Bullister, J.L., Key, R.M., Peng, T.H., Kozyr, A., Ono, T., Wong, C.S., 2002. In situ calcium carbonate dissolution in the Pacific Ocean. Global Biogeochem. Cycles 16 (4), 1144, doi:10.1029/2002GB001866.

Gardner, W.D., Walsh, I.D., Richardson, M.J., 1993. Biophysical forcing of particle production and distribution during a spring Bloom in the North Atlantic. Deep-Sea Research II 40, 171-195.

Gardner, W. D., Richardson, M. J., Carlson, C. A., Hansell, D., Mishonov, A. V. 2003. Determining true particulate organic carbon: bottles, pumps and methodologies. Deep-Sea Research II 50, 655–674.

Gardner, W.D., Mishonov, A.V., Richardson, M.J. (2006), Global POC concentrations from in-situ and satellite data. Deep-Sea Research II 53, 718–740.

Gehlen, M., Bopp, L., Emprin, N., Aumont, O., Heinze, C., and Ragueneau, O. (2006) Reconciling surface ocean productivity, export fluxes and sediment composition in a global biogeochemical ocean model. Biogeosciences 3, 521-537.

Gilbert, O.M. and Buskey E.J., 2005. Turbulence decreases the hydrodynamic predator

sensing ability of the canaloid copepod Acartia tonsa. J. Plankton Res. 27, 1067-1071.

Honda, M. C., Imai, K., Nojiri, Y., Hoshi, F., Sugawara, T., Kusakabe, M., 2002. The biological pump in the northwestern North Pacific based on fluxes and major components of particulate matter obtained by sediment trap experiments (1997-2000). Deep-Sea Research II 49, 5595-5625.

Jackson, G.A., and Burd, A. B., 2002. A model for the distribution of particle flux in the mid-water column controlled by subsurface biotic interactions. Deep-Sea Research II 49, 193–217.

Karl, D.M., and Knauer, G.A., 1985. Vertical distribution, transport, and exchange of carbon in the northeast Pacific Ocean: evidence for multiple zones of biological activity. Deep-Sea Research, 31, 221-243.

Karl, D.M., Christian, J.R., Dore, J.E., Hebel, D.V., Letelier, R.M., Tupas, L.M., Winn, C.D., 1996. Seasonal and interannual variability in primary production and particle flux at Station ALOHA. *Deep-Sea Research II* 43 (2-3), 539-568.

Kobari , T., Steinberg, D.K., Ueda, A., Tsuda, A., Silver, M.W., Kitamura, M., 2008. Impacts of ontogenetically migrating copepods on downward carbon flux in the western subarctic Pacific Ocean. Deep-Sea Research II.

Lam, P.J., Bishop, J.K.B., 2007. High Biomass Low Export Regimes in the Southern Ocean. *Deep-Sea Research II* 54, 601–638.

Lam, P.J., Bishop, J.K.B., 2008. The Continental Margin is a Key Source of Iron to the HNLC North Pacific Ocean. *Geophys. Res. Lett.* 35, L07608, doi:10.1029/2008GL033294.

Lamborg, C.H., Buesseler, K.O., Valdes, J., Bertrand, C.H., Bidigare, R., Manganini, S., Pike, S., Steinberg, D., Trull, T., Wilson, S., 2008. The Flux of Bio- and Lithogenic Material Associated with Sinking Particles in the Mesopelagic "Twilight Zone" of the Northwest and North Central Pacific Ocean. *Deep-Sea Research II.*

Lampitt, R.S., Wishner, K.F., Turley, C.M. and Angel, M.V., 1993. Marine snow studies in the Northeast Atlantic Ocean: distribution, composition and the role oas a food source for migrating plankton. Marine Biology 116, 689-702.

Liu, G. Stewart, Cochran, J.K., Lee, C., Armstrong, R.A., Hirschberg, D.J., Gasser B. and Miquel, J.-C., 2005, Why do POC concentrations measured using Niskin bottle collections sometimes differ from those using in-situ pumps?, *Deep-Sea Res. I* 52, 1324–1344.

Nelson, D.M., Treguer, P., Brzezinski, M.A., Leynaert, A., and Queguiner, B., 1995. Production and dissolution of biogenic silica in the ocean: Revised global estimates, comparisons with regional data and relationship to biogenic sedimentation. Global Biogeochemical Cycles 9, 359-372.

Sabine, C.L., Mackenzie, F.T., Winn, C., and Karl, D.M. 1995. Geochemistry of carbon dioxide in seawater at the Hawaii Ocean Time series station, ALOHA. Global Biogeochemical Cycles, 9, 637-651.

Siegal, D.A., Dickey, T.D., Washburn, L., Hamilton, M.K., Mitchell, B.K., 1989. Optical determination of particulate abundance and production variations in the oligotropic ocean. Deep-Sea Research 36, 211-222.

Siegel, D.A., Fields, E., Buesseler, K.O., 2007. A bottom-up view of the biological pump: Modeling source funnels above ocean sediment traps. Deep Sea Research I, submitted.

Steinberg, D.K., Cope, J.S., Wilson, S.E., Kobari, T., 2008. A comparison of mesopelagic zooplankton community structure in the subtropical and subarctic North Pacific Ocean. *Deep-Sea Research II*.

Turnewitsch, R., Springer, B. M., Kiriakoulakis, K., Vilas, J. C., Arístegui, J., Wolff, G., Peine, F., Werk, S., Graf, G., Wanie, J. J., 2007. Determination of particulate organic carbon (POC) in seawater: The relative methodological importance of artificial gains and losses in two glass-fiber-filter-based techniques. Marine Chemistry 105, 208 – 228

Volk, T., Hoffert, M.I., 1985. Ocean carbon pumps: Analysis of relative strengths and

efficiencies in ocean-driven atmospheric CO_2 changes. Geophysical Monographs 32, 99-110.

Walsh, I.D., Chung, S.P., Richardson, M.J., Gardner, W.D., 1995. The diel cycle in the integrated particle load in the equatorial Pacific: a comparison with primary production. Deep-Sea Research II 42, 465-479.

Wilson, S.E., Steinberg, D.K., Buesseler, K.O., 2008. Changes in fecal pellet characteristics with depth as indicators of zooplankton repackaging of particles in the mesopelagic zone of the subtropical and subarctic North Pacific Ocean. *Deep Sea Research II.*

Table 1 MULVFS Particulate Matter Chemistry at Station ALOHA: Organic Carbon, Phosphorus, Inorganic Carbon, and Silicon.

	POC (nM)				PP (pM)				PIC (nM)		PSi (μM)	
Depth	<1 μm[A]	1-51 μm[B]	<1+1-51 μm[C]	>51 μm[D]	<1 μm	1-51 μm	>51 μm	>0.4 μm[E]	<51 μm[F]	>51 μm	>51 μm	>0.4 μm[E]
MULVFS Cast 1 (D1)	*Day 175.867 to 176.035*				*158.048°W, 22.724°N to 158.045°W, 22.727°N*			*ctd 20,21*				
30	224 ± 6	856 ± 6	1080 ± 8	175	1385	4099	3258 ± 288	5175 ± 592	23.1	8.3 ± 2.0	15.2 ± 0.1	41.3
55	236 ± 5	932 ± 5	1168 ± 8	70 [c]		4251	1305 ± 222	3918 ± 430	27.5	7.6 ± 1.3	14.4 ± 0.3	25.9
80	180 ± 4	623 ± 4	803 ± 6	40 [c]	1341	3330	705 ± 29		27.1	6.9 ± 0.5	10.4 ± 0.2	15.4
105	164 ± 4	541 ± 4	704 ± 5	64	1181	3146	1115 ± 85	2440 ± 256	23.9	7.0 ± 1.2	7.6 ± 0.4	15.5
155	58 ± 3	312 ± 3	369 ± 4	60	595	1864	449 ± 33	2133 ± 269	29.9	7.0 ± 0.7	4.2 ± 0.3	13.8
205	30 ± 2	207 ± 2	238 ± 3	26 [c]	349 ± 4	1059 ± 25	194 ± 0		22.5 ±1.0	3.1 ± 0.3	2.8 ± 0.2	6.2
255	20 ± 2	205 ± 2	225 ± 3	16 [c]	255 ± 21	899 ± 40	136 ± 19		27.2 ±1.8	3.5 ± 0.4	2.5 ± 0.2	8.4
330	29 ± 2	115 ± 2	144 ± 3	14	177	718	118 ± 14	440 ± 129	33.0	3.5 ± 0.4	1.7 ± 0.3	5.9
480	21 ± 2			14	136	548	93 ± 13		32.2	3.8 ± 0.4	1.6 ± 0.2	6.8
680	7 ± 2	99 ± 2	107 ± 2	3.5[c]	69	440	23 ± 9	284 ± 100	31.3	1.6 ± 0.2	0.9 ± 0.2	9.2
830	13 ± 2	86 ± 2	99 ± 3	4.4[c]	105 ± 0	383 ± 6	29 ± 9	256 ± 97	28.9 ±0.0	1.5 ± 0.2	0.7 ± 0.2	9.2
MULVFS Cast 2 (D1)	*Night 178.352 to 178.519*				*158.094°W, 22.699°N to 158.085°W, 22.702°N*			*ctd 29, 30*				
30	110 ± 6	761 ± 6	871 ± 8	231	941	4038	1484 ± 69		24.2	7.1 ± 1.7	12.8	13.1
54	147 ± 5	842 ± 5	989 ± 8	140 [c]	1137	4689	897 ± 61		26.3	11.7 ± 2.6	11.7	20.4
79	117 ± 4	585 ± 4	701 ± 6	190 [c]	943	3398	732 ± 58		27.3	9.1 ± 1.6	5.9	17.0
104	85 ± 3	404 ± 3	489 ± 5	157	1227	2627	603 ± 30	3933 ± 262	19.7	6.7 ± 0.9	6.1	
153	65 ± 2	306 ± 2	371 ± 4	86	658	2062	294 ± 18	3266 ± 241	44.3	6.9 ± 0.9	4.8	16.2
202	30 ± 2	202 ± 2	232 ± 3	95 [c]	383	1337	326 ± 22	1174 ± 155	22.5	4.5 ± 0.6	2.7	10.1
252	14 ± 2	143 ± 2	157 ± 3	16 [c]	247 ± 7	914 ± 78	162 ± 18		30.5 ±2.6	5.3 ± 0.6	2.6	12.3
326	6 ± 2	141 ± 2	147 ± 3	18	249	786	187 ± 7	729 ± 119	31.9	6.4 ± 0.7	2.3	7.6
474	7 ± 2	122 ± 2	129 ± 3	16	135	714	61 ± 9	666 ± 128	38.5	3.6 ± 0.4	1.1	5.8
572	2 ± 2	110 ± 2	111 ± 2	8 [c]	81	528	32	601 ± 101	35.9	3.0	1.2	8.8
770	6 ± 2	87 ± 2	93 ± 2	9 [c]	65	449	36 ± 5		29.5	2.5 ± 0.2	1.0	6.9
MULVFS Cast 3 (D2)	*Day 186.828 to 186.999*				*157.996°W, 22.752°N to 157.992°W, 22.750°N*			*ctd 81, 82*				
30	b	b	b		1288 ± 55	5810 ± 499	1205 ± 144	6247 ± 540	24.7 ±3.0	7.2 ± 1.8	24.3	21.0
55	b	b	b		1172 ± 54	5534 ± 8	1471 ± 169	3822 ± 273	23.9 ±2.0	9.6 ± 1.5	24.9 ± 9.6	15.0
80	b	b	b		1020 ± 9	4789 ± 111	1818 ± 161		28.5 ±1.9	13.2 ± 1.7	16.5	10.5
104	b	b	b		1780 ± 14	2865 ± 188	1228 ± 202	3215 ± 233	20.2 ±2.1	7.5 ± 0.8	14.7	10.7
154	b	b	b		607 ± 17	1881 ± 43	404 ± 38		37.2 ±2.0	7.8 ± 0.8	6.5	8.3
204	b	b	b		393 ± 8	1227 ± 34	121 ± 9	1483 ± 117	23.8 ±1.6	3.4 ± 0.3	3.0	5.2
254	b	b	b		263 ± 8	868 ± 25	67 ± 12		30.1 ±2.1	3.2 ± 0.3	2.4	7.1
328	6 ± 2	132 ± 2	138 ± 3		212 ± 5	638 ± 97	45 ± 9		28.8 ±2.2	2.3 ± 0.3	1.0	5.3
676	6 ± 2	100 ± 2	106 ± 2		79	443	(-1)		26.2	1.0	0.8	7.2
825	1 ± 2	102 ± 2	104 ± 2		58	397	16 ± 4	344 ± 95	26.4	1.0 ± 0.2	0.7	6.9

MULVFS Cast 4 (D2)	*Night 187.351 to 187.520*				*158.001°W, 22.751°N to 157.997°W, 22.749°N*			*ctd 83*				
30	154 ± 6	951 ± 6	1105 ± 8	274	1208	6314	1359 ± 107		30.6	10.1 ± 2.2	12.6 ± 0.5	18.5
54	227 ± 6	1058 ± 6	1285 ± 8	253 [c]	1113	5792	1257 ± 86		30.9	13.9 ± 1.8	22.2 ± 0.2	19.5
79	143 ± 4	573 ± 4	715 ± 6	108 [c]	1058	4426	862 ± 94		30.1	10.6 ± 1.5	14.0 ± 2.5	35.5
103	152 ± 3	545 ± 3	698 ± 4	104	1603	3422	829 ± 63		30.8	9.8 ± 1.2	9.4 ± 0.5	11.1
202	25 ± 2	165 ± 2	191 ± 3	62	531	1187	117 ± 8		21.8	4.1 ± 0.5		6.3
251	26 ± 2	126 ± 2	153 ± 3	86 [c]	331	1176	163 ± 9	1201 ± 118	32.3	4.3 ± 0.4	2.3	5.9
325	20 ± 2	75 ± 2	95 ± 3	30 [c]	199	896	40 ± 2		37.4	2.7 ± 0.4	1.9	4.2
472	18 ± 2	74 ± 2	93 ± 3	18	166	743	24 ± 3	733 ± 111	37.3	1.8 ± 0.1	1.0	5.0
571	8 ± 2	104 ± 2	112 ± 2	17	101	608	19 ± 3		35.2	2.3 ± 0.3	1.4	3.7
768	5 ± 2	94 ± 2	100 ± 2	16 [c]	82	543	18 ± 4		32.2	1.5 ± 0.2	0.8	7.0
MULVFS Cast 5 (D2)	*Day 189.839 to 190.007*				*158.243°W, 22.752°N to 158.241°W, 22.751°N*			*ctd 95, 96*				
22	137 ± 5	790 ± 5	928 ± 7		912	4010	1734 ± 83	6366 ± 423	15.7	8.2 ± 1.6	8.7	12.3
122	104 ± 3	437 ± 3	541 ± 4	98 [c]	901	2466	677 ± 25		57.2	16.1 ± 1.5	7.8	13.1
172				49	469	1610	340 ± 31		18.4	7.5 ± 0.9	4.4	5.8
222	25 ± 2	162 ± 2	186 ± 3	24 [c]	368	1021	167 ± 11		20.3	5.1 ± 0.9	2.8	8.1
272	20 ± 2	107 ± 2	127 ± 2		196 ± 2	765 ± 36	108 ± 11	1217 ± 141	20.6 ±1.3	4.3 ± 0.5	2.2	5.6
322					183	823	108 ± 8	1126 ± 118	30.2	3.9 ± 0.4	2.1	3.3

Cast information: local day or night, decimal UTC day and station positions at start and end of sampling, respectively, and CTD casts near time of sampling

A,B - MAIN WHATMAN QMA (WHOI: Total Particulate Carbon (PC) corrected for PIC in individual bottom and top samples), error indicates uncertainty of blank correction;

C - MAIN WHATMAN QMA (Sum of A and B), error indicates uncertaity of blank correction;

D - POC (PC corrected for PIC) rinsed from 53 μm TETKO Polyester filter [Trull Holder, WHOI anal.].

E - SIDE ARM 0.4 μm Poretics filter.

F - PIC - Particulate Inorganic Carbon from ICP-MS Ca [seawater corrected] on QMA combined top and bottom samples). Errors are replicate analyses;

a POC PN ratios indicate sample was left wet and organics were lost prior to analysis;

b. samples lost;

c. [ ] >51 μm C_{org} estimated based on >51μm P and C_{org}/P of nearest sample.

blank entry means analysis not performed.

Table 2 MULVFS Particulate Matter Chemistry at Station K2: Organic Carbon, Phosphorus, Inorganic Carbon, and Silicon.

	POC (nM)				PP (pM)				PIC (nM)		PSi (μM)	
Depth	<1 μm[A]	1-51 μm[B]	<1+1-51 μm[G]	>51 μm[H]	<1 μm	1-51 μm	>51 μm	>0.4 μm[E]	<51 μm[F]	>51 μm	>51 μm	>0.4 μm[E]
MULVFS Cast 7 (D1), Day 211.710 to 212.175 161.010°E,47.001°N ctd 18, 19												
10	752 ± 24[a]	1891 ± 24[a]	2758 ± 61	993 ± 3	5210	12510	14408		32.8 ± 4.0	52.6	1318	2173
35	380 ± 26[a]	1074 ± 26[a]	2389 ± 66	1372 ± 3	5102	11118	16638		56.8 ± 8.7	86.5	1575	2994
60	176 ± 16[a]	820 ± 16[a]	1590 ± 41	685 ± 2	2490 ± 22	7019 ± 519	4100	7391 ± 158	22.3 ± 2.9	21.4	369	790
85	95 ± 10[a]	375 ± 10[a]	779 ± 26	206 ± 1	1155	3575	1832		18.2 ± 1.2	12.7	199	350
135	91 ± 11[a]	476 ± 11[a]	688 ± 27	153 ± 1	634	3356	929 ± 33		22.5 ± 0.2	8.3 ± 0.6	106	395
185	40 ± 12[a]	367 ± 12[a]	627 ± 29	126 ± 1	606	3329	512 ± 12		32.0 ± 2.9	7.8 ± 1.0	102	546
235	42 ± 12[a]	398 ± 12[a]	635 ± 30	127 ± 1	461	2349	702 ± 208		20.2 ± 1.0	7.3 ± 0.1	118	796
310	46 ± 9[a]	281 ± 9[a]	428 ± 23	86 ± 1	383	1848	288 ± 13		20.1 ± 1.6	4.3 ± 0.1	105	606
460	45 ± 7[a]	210 ± 7[a]	305 ± 19	45 ± 1	258 ± 6	1198 ± 30	251 ± 61	1230 ± 65	17.9 ± 0.5	4.8 ± 0.1	60	305
560	39 ± 7[a]	209 ± 7[a]	267 ± 17	77 ± 1	265	1069	139 ± 14		15.6 ± 0.1	4.5 ± 0.4	52	128
760	17 ± 6[a]	131 ± 6[a]	206 ± 14	25 ± 1	176	1040	108	588 ± 40	18.0 ± 3.5	3.1	32	147
MULVFS Cast 8 (D1), Night 213.421 to 213.614 161.000°E,47.000°N ctd 22,23												
10	220 ± 27[a]	712 ± 27[a]	2604 ± 67	2654 ± 3	5972	17153	25443	26971 ± 479	32.2	37.9	1846	2593
35	309 ± 32[a]	1124 ± 32[a]	3322 ± 81	1297 ± 4	7278	21375	11603		90.6	63.1	1661	2579
60	98 ± 19[a]	455 ± 19[a]	1676 ± 49	324 ± 2	2561	7565	4229	7616 ± 147	19.5	16.3	398 ± 26	770
85	62 ± 13[a]	312 ± 13[a]	902 ± 32	255 ± 1	2032	4708	1989		15.9	8.3	233	744
135	39 ± 11[a]	257 ± 11[a]	674 ± 28	140 ± 1	987 ± 47	4002 ± 32	1439	3051 ± 110	24.5 ± 2.0	8.9	199	468
185	50 ± 10[a]	197 ± 10[a]	548 ± 24	111 ± 1	792	3020	627		27.6	8.3	174	393
235	44 ± 11[a]	218 ± 11[a]	536 ± 27	457 ± 1	524	2772	473		29.4	8.6	142	612
310	46 ± 9[a]	217 ± 9[a]	356 ± 23	52 ± 1	538	2037	507 ± 95		18.8	7.5 ±0.4	108	568
460	34 ± 7[a]	163 ± 7[a]	351 ± 18	32 ± 1	376	1503	177	1114 ± 68	21.6	4.5	70	236
660	18 ± 6[a]	112 ± 6[a]	215 ± 15	23 ± 1	216	1371	250 ± 2		18.6	5.4 ±0.3	67	142
810	19 ± 5[a]	101 ± 5[a]	282 ± 14	15 ± 1	221	1040	161	612 ± 52	17.5	3.7	42	
MULVFS Cast 9 (D2), Day 223.036 to 223.224 161.000°E, 47.050°N ctd 63, 64												
10	406 ± 19	1485 ± 19	2506 ± 48	1205 ± 2	4896 ± 46	11916 ± 131	8328	20197 ± 412	8.1 ± 0.1	22.0	384 ± 33	730
34	327 ± 22	1381 ± 22	2238 ± 55	378 ± 2	4779	10942	2941		10.1	13.0	280 ± 11	1203
59	171 ± 19	1010 ± 19	1547 ± 47	108 ± 2	2684	8453	728	9375 ± 201	13.6	2.6	120	892
84	134 ± 16	746 ± 16	997 ± 39	150 ± 2	2029	5434	612		9.9	2.0	119	819
134	55 ± 14	596 ± 14	815 ± 34	94 ± 2	987	3925	638	3211 ± 119	11.8	2.6	112	952
184	59 ± 13	556 ± 13	713 ± 33	34 ± 1	1093	3489	428		12.7	1.2	98	1024
234	56 ± 13	478 ± 13	542 ± 33	102 ± 2	806	3418	230	4377 ± 134	14.0	2.4	136	1038
309	36 ± 9	289 ± 9	452 ± 23	101 ± 1	573 ± 34	2218 ± 66	547		13.4 ± 0.3	3.4	110	415
458	27 ± 7	219 ± 7	295 ± 18	35 ± 1	310 ± 9	1327 ± 72	148	1175 ± 61	15.4 ± 0.5	2.8	70	318
558	21 ± 7	200 ± 7	274 ± 17	34 ± 1	242 ± 27	1434 ± 122	246		13.5 ± 1.1	3.2	52	384
758	13 ± 6	176 ± 6	242 ± 15	20 ± 1	239 ± 17	1201 ± 69	82	1293 ± 56	17.6 ± 1.3	2.6	42	172

MULVFS Cast 10 (D2), Night 224.441 to 224.628 161.000°E, 47.050°N ctd 65,66

10	475 ± 17	1730 ± 17	2350 ± 44	2807 ± 2	5639	13713	16437		7.2	18.1	267	619
35	474 ± 19	1619 ± 19	2455 ± 49	452 ± 2	5693	14137	4524 ± 80	7032 ± 302	6.6	22.9 ± 1.7	497	675
60	309 ± 21	1522 ± 21	2097 ± 53	80 ± 2	3816	11967	767		9.6	1.8	119	1105
85	138 ± 16	978 ± 16	1115 ± 41	168 ± 2	2213 ± 75	5095	893	4346 ± 125	5.6	1.1	182	803
135	73 ± 13	665 ± 13	736 ± 33	93 ± 2	1065 ± 39	4243 ± 74	745		8.1 ± 3.4	3.4	124	1004
185	140 ± 13	532 ± 13	649 ± 32	62 ± 1	941 ± 52	3922 ± 48	508	3030 ± 106	12.9 ± 1.9	1.9	111	320
235	77 ± 12	437 ± 12	570 ± 31	396 ± 1	846	3249	401		14.4	2.6	131	319
310	40 ± 9	307 ± 9	393 ± 23	62 ± 1	628	2441	474	3520 ± 124	16.4	2.0	101	329
385	49 ± 8	293 ± 8	354 ± 20	103 ± 1	435	1703	269		14.2	2.6	98	267
660	40 ± 6	192 ± 6	245 ± 15	46 ± 1	255	1080	124	1014 ± 52	15.0	3.0	51	99
810	38 ± 6	177 ± 6	242 ± 15	22 ± 1	259 ± 35	1097 ± 112	131		18.0 ± 1.7	3.5	45	169

Cast information: local day or night, decimal UTC day and station positions at start and end of sampling, respectively, and CTD casts near time of sampling.
Single position report implies no change of location during sampling.
A,B - MAIN WHATMAN QMA (WHOI: Total Particulate Carbon (PC) corrected for PIC in individual bottom and top samples), error indicates uncertainty of blank correction;
D - TRULL HOLDER 53 μm POLYESTER (WHOI: PC corrected for PIC of particles rinsed from prefilter).
E - SIDE ARM Sample 0.4 μm Poretics filter
F - PIC - Particulate Inorganic Carbon from ICP-MS Ca [seawater corrected] on QMA combined top and bottom samples). Errors are replicate analyses;
G - MAIN WHATMAN QMA. (UTAS: POC analysis of combined top and bottom QMA filters, after acid fuming);
H - MAIN 53 μm POLYESTER (UTAS: POC analysis of particles rinsed from 1/8th of MAIN prefilter sample; after acid fuming).
a. POC/PN ratios indicate sample was left wet and organics were lost prior to analysis;
b. samples lost;
blank entry means analysis not performed.

Bishop/Wood Figure Captions

Fig. 1. Map showing locations of summertime VERTIGO studies at ALOHA (2004) and K2 (2005) and isolines of mean surface dissolved nitrate (in μM) redrawn from Buesseler et al. (2008). Land outlines and 1000 m isobath contours are also depicted.

Fig. 2. A. MULVFS pump shown attached to the polyurethane coated electromechanical cable. Filter holders are protected with plastic until seconds prior to deployment. B. Flow logic and configuration of three separately metered flow paths: (1) Main filter holder. (2) Auxillary flow path shown occupied by a filter holder assembly provided by T. Trull. Absorber cartridges were also added in-line as illustrated. (3) "Side arm" flow path. Used for of up to six 47 mm filter holders. (C) Exploded view of main filter holder indicating filters and baffle assemblies.

Fig. 3. Profiles of particle beam attenuation coefficient (C_P) during ALOHA CTD cast 21 (left) and during K2 CTD cast 22 (right). These profiles were near local dusk just after completion of MULVFS casts 1 and 7, respectively. The blue (or dark) curves are 24 Hz down-cast C_P data without any filtering to remove spikes. The orange (or lighter) curve represents the spike-free profile. We use the despiked data for POC time series at both locations (Fig. 9).

Fig. 4. Winds (m s^{-1}), short wave irradiance (SWR, W m^{-2}), sea surface temperature (SST, °C), and mixed layer depth ($MLD_{0.05}$) at K2 during VERTIGO. Vertical bars at the

bottom of the plot denote timing of MULVFS casts M07, M08, M09, and M10. Horizontal bars at top and bottom of the graph denote intensive study periods K2-D1 and K2-D2. The scale is in days (UTC time, 2005).

Fig. 5. Temperature timeseries for upper 550 m at ALOHA and K2. The red curve at the bottom the two lower panels denotes distance (in km) from centers of studies at ALOHA (22.75°N, 155°W) and near K2 (47°N, 161°W). Gray vertical bars denote times of MULVFS sampling. The small orange triangles denote times of CTD-rosette casts. Heavy solid lines correspond to 5°C, 10°C, 15°C, 20°C, and 25°C isotherms. Temperature is contoured at 1 degree intervals for waters colder than 15 °C. Heavy dashed lines denote the 2 °C isotherm and the temperature minimum zone at K2. Horizontal colored bars correspond to ALOHA D1 and D2, and K2 D1 and D2 intensive study periods. Yellow bars depict NBST deployments. Red/white bars on the K2 plot depict optical sedimentation recorder deployments (not discussed in this paper).

Fig. 6. Abundance profiles of copepods, chaetognaths, siphonophores and colonial radiolaria captured on 51 μm MULVFS prefilters at station K2. Copepod abundances at 10 m in the turbulent mixed layer were approximately 18% those reported from corresponding 0-50 m IONESS tows (Steinberg et al., 2008); only several percent of copepods were sampled by MULVFS in deeper waters. Abundance profiles of slow-swimming siphonophores and of non-swimming colonial radiolaria match Steinberg et al. (2008) data.

Fig. 7. Dependence of particle beam attenuation coefficient (C_P) sensitivity on transmissometer receiver acceptance angle (RAA). Bracketing C_P profiles from the (1.5° RAA) WETLabs C-Star transmissometer were compared to deployment and recovery profiles taken using a (0.92° RAA) WETLabs C-Rover transmissometer during cast M08. 18% differences in sensitivity were found.

Fig.8. (A and B) Comparion of Dawn/Dusk POC_{Cp} profiles with total POC determined using MULVFS at ALOHA and K2. (C and D) Seapoint turbidity sensor profiles scaled upwards by a factor of 80 to match POC at 310 m. The POC vs. POC_{Cp} estimates are a much closer match. Zooplankton captured by MULVFS contributed an estimated 0.9 μM (night) and 0.2 μM (day) POC at 10 m at K2.

Fig. 9. Time series of POC_{Cp} occupations of ALOHA (left panels) and K2 (right panels). Inverted triangles at the top of each panel mark the times of CTD casts. The white curve denotes $MLD_{0.05}$, the mixed layer depth. The red curve is distance (in km) from center of studies at ALOHA and K2. Yellow horizontal bars denote NBST depths and deployment times (Buesseler et al. 2008, Lamborg, et al., 2008).

Fig. 10. Daily variations of mixed layer POC_{Cp} at ALOHA showing a 25% diurnal fluctuation of particle concentration (high at dusk; low at dawn). This reflects a near steady state balance between primary production and grazing. MULVFS sample collection times are also shown. The curve is a polynomial trend line fit to the results.

Fig. 11. Time series of turbidity (mFTU) during VERTIGO ALOHA and K2 studies. Inverted orange triangles, red curves, and gray vertical bars as for Fig 9. At K2, scattering decreased in both near surface and deeper waters over time.

Fig. 12. A. Profiles of spike C_P (left) and turbidity (right) anomaly averaged over 20 m intervals for ALOHA and K2. The blue (or darkest) line depicts the averages of all casts within 30 km of station ALOHA. Spikes are largely absent from ALOHA profiles below 200 m. The red (darker line with up triangles) and green (lighter line with down triangles) profiles correspond to separately pooled K2 cast data collected during D1 and D2 periods. B. Abundance profiles of spikes (# m^{-3}) lasting >0.1 seconds (heavy lines) and >0.3 seconds (thin lines) in transmissometer and turbidity (scattering sensor) profiles on down-casts of the CTD. CTD lowering speeds were 30-40 cm s^{-1} and 90-100 cm s^{-1} above and below 100m, respectively. Larger graphs are K2 data. Inserted small graphs depict ALOHA data. The structure of profiles spike C_P anomaly and abundances match closely the depth systematics of zooplankton biomass and abundance (Steinberg et al., 2008). Scattering spike profiles do not show the strong minimum in the temperature minimum zone and are more likely to reflect abundances of larger and chained phytoplankton/ microzooplankton and aggregate particles. The changes between K2-D1 and K2-D2 in the surface layer closely parallel trends in >51 μm Si (Fig. 16).

Fig. 13. Profiles of <1, 1-51, and >51 μm POC (C_{org}) and P in MULVFS samples. Data from individual casts are represented by symbols. In the case of ICP-MS measured P, error bars shown associated with a symbol represent replicate analyses of the sample

during multiple analysis runs. Blue (darkest in black and white), red (medium dark), and green (lightest) lines represent averages of data from ALOHA (M01 through M04), K2-D1 (M07 and M08), and K2-D2 (M09 and M10), respectively.

Fig. 14. Profiles of C_{org}/N in combined <1 and 1-51 μm particle size fractions and >51 μm fractions. Error bars denote contributions of blank correction and analytical error to the assigned ratios. Blue (darkest in black and white), red (medium dark), and green (lightest) lines represent averages of data from ALOHA K2-D1, and K2-D2, respectively.

Fig. 15. Profiles of 1-51 and >51 Ca^* (Ca corrected for seasalt) and >0.4 μm (Side Arm) and >51 μm Si at ALOHA and K2 sites. The >0.4 μm Si includes particles in the >51 μm fraction. Symbols and lines are drawn as in previous figures. Major losses of both >51 and 1-51 μm Ca^* occurred between K2-D1 and K2-D2. Abundances of Si were a factor of ~100 greater at K2 than at ALOHA.

Fig. 16. Profiles of 1-51 and > 51 μm Sr, Ba and Mn at ALOHA and K2. Notable were the high concentrations of >51 μm Sr at ALOHA in surface waters which reflected high abundances of Acantharia. Symbols and lines are drawn as in previous figures. The 1-51 μm Mn data indicate lateral delivery of Mn oxides from reducing continental margin sediments (Lam and Bishop, 2008). This material, incorporated during particle repackaging processes, is seen in the collections of 300 m and 500 m NBSTs (Lamborg et al., 2008). Notable is the observation that >51 μm Mn in the euphotic layer far exceeds (especially at 10 m) levels seen in the 1-51 μm fraction. This suggests a net upward

transport of metals captured by zooplankton feeding near 150 m during their diurnal migrations.

Fig. 17. Depth integrated 1-51 and >51 μm stocks of Ca^* and Si, and Ba for K2-D1 and K2-D2 periods. Integrations were performed upwards from 800 m to the surface. Red (darker) and green (lighter) lines denote the mean profiles for D1 and D2, respectively.

Fig. 18. Budgets for carbonate and Si particles at ALOHA and K2. Large symbols: production of PIC and Si estimated using Boyd et al. (2008) size fractionated primary productivity data and MULVFS data. NBST data are from Lamborg et al. (2008). ΔS denotes net change in suspended particle stocks between K2-D1 and K2-D2. Over 92% percent of carbonate particles produced and present at K2 were dissolved in the upper 500 m. Little particulate carbonate dissolution was apparent at ALOHA. Approximately 50% and 65% of the Si dissolved at ALOHA and K2 above 500 m.

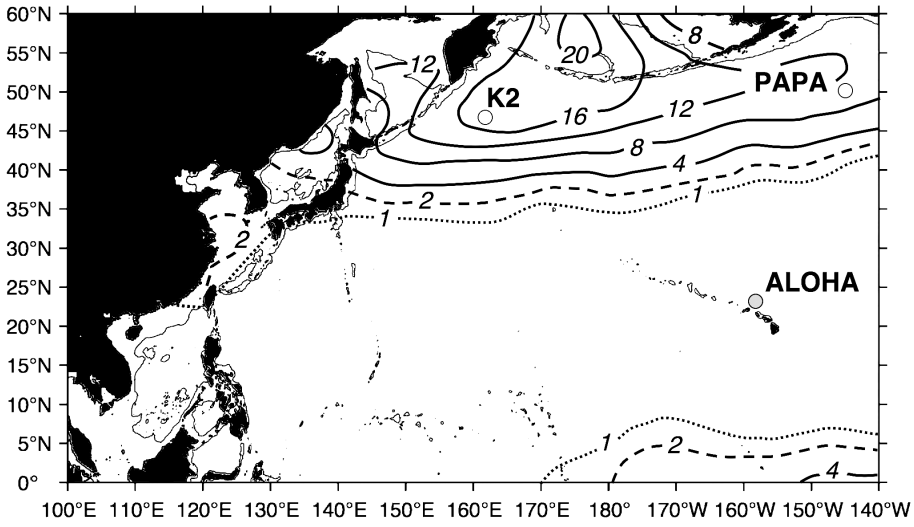
60°N
55°N
50°N
45°N
40°N
35°N
30°N
25°N
20°N
15°N
10°N
5°N
0°
100°E 110°E 120°E 130°E 140°E 150°E 160°E 170°E 180° 170°W 160°W 150°W 140°W
K2
PAPA
ALOHA
12
20
8
16
12
8
4
2
1
2
1
1
2
4

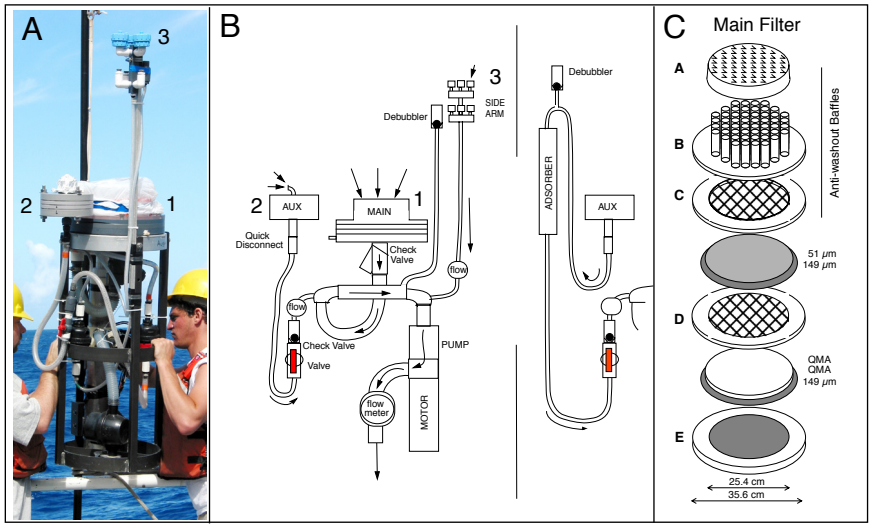
A
3
2
1
B
3
SIDE ARM
Debubbler
2
AUX
MAIN
1
Quick Disconnect
Check Valve
flow
flow
Check Valve
Valve
PUMP
flow meter
MOTOR
Debubbler
ADSORBER
AUX
C
Main Filter
A
B
C
D
E
Anti-washout Baffles
51 μm
149 μm
QMA
QMA
149 μm
25.4 cm
35.6 cm

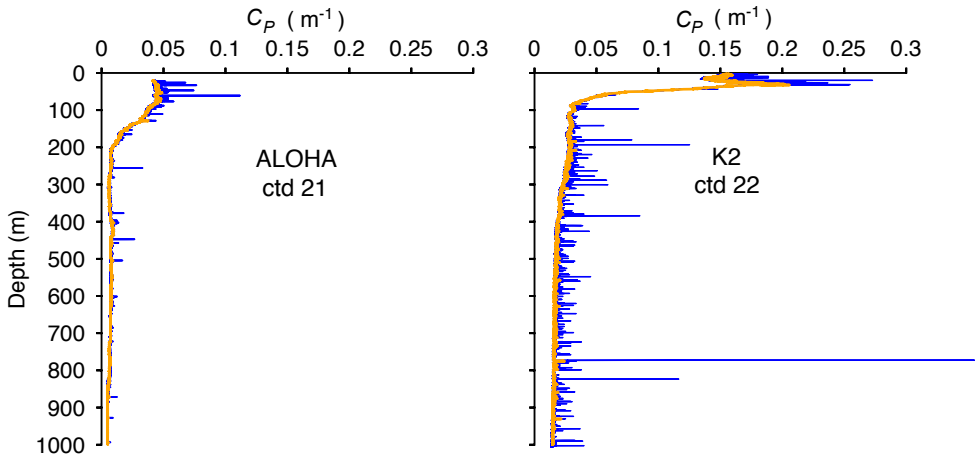
C_P (m^{-1})
0
0.05
0.1
0.15
0.2
0.25
0.3
Depth (m)
0
100
200
300
400
500
600
700
800
900
1000
ALOHA
ctd 21
K2
ctd 22

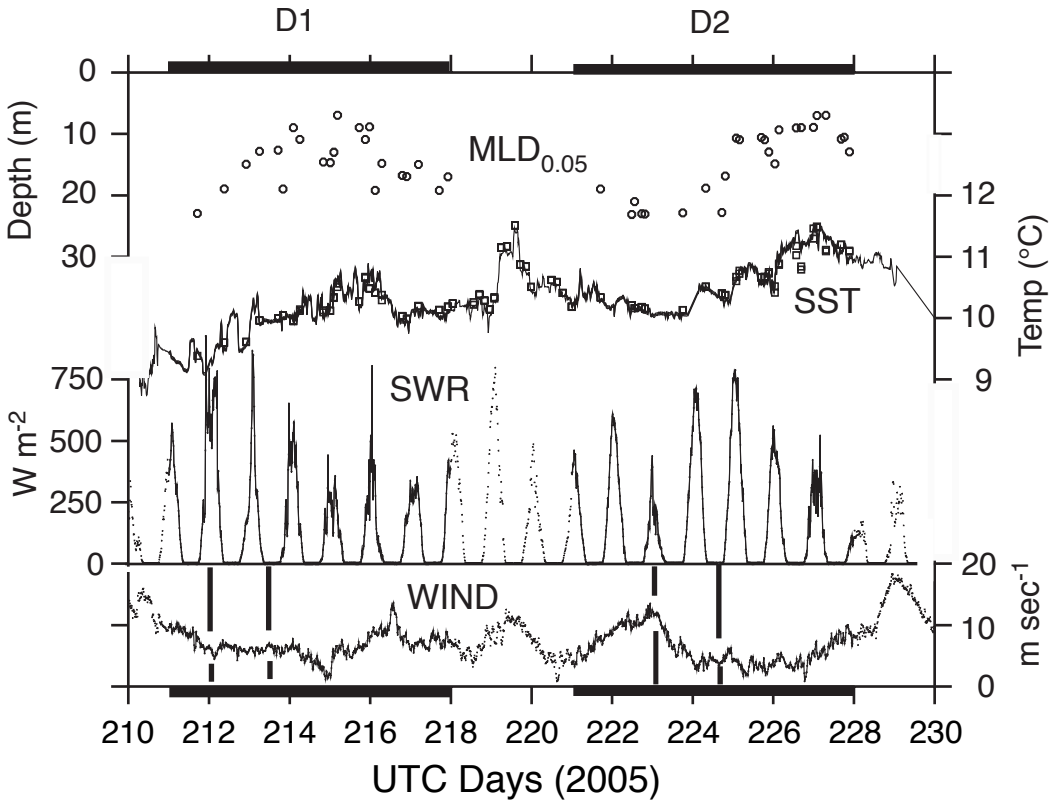
D1
D2
Depth (m)
0
10
20
30
MLD0.05
12
11
10
9
Temp (°C)
SST
750
500
250
0
W m-2
SWR
20
10
0
m sec-1
WIND
210
212
214
216
218
220
222
224
226
228
230
UTC Days (2005)

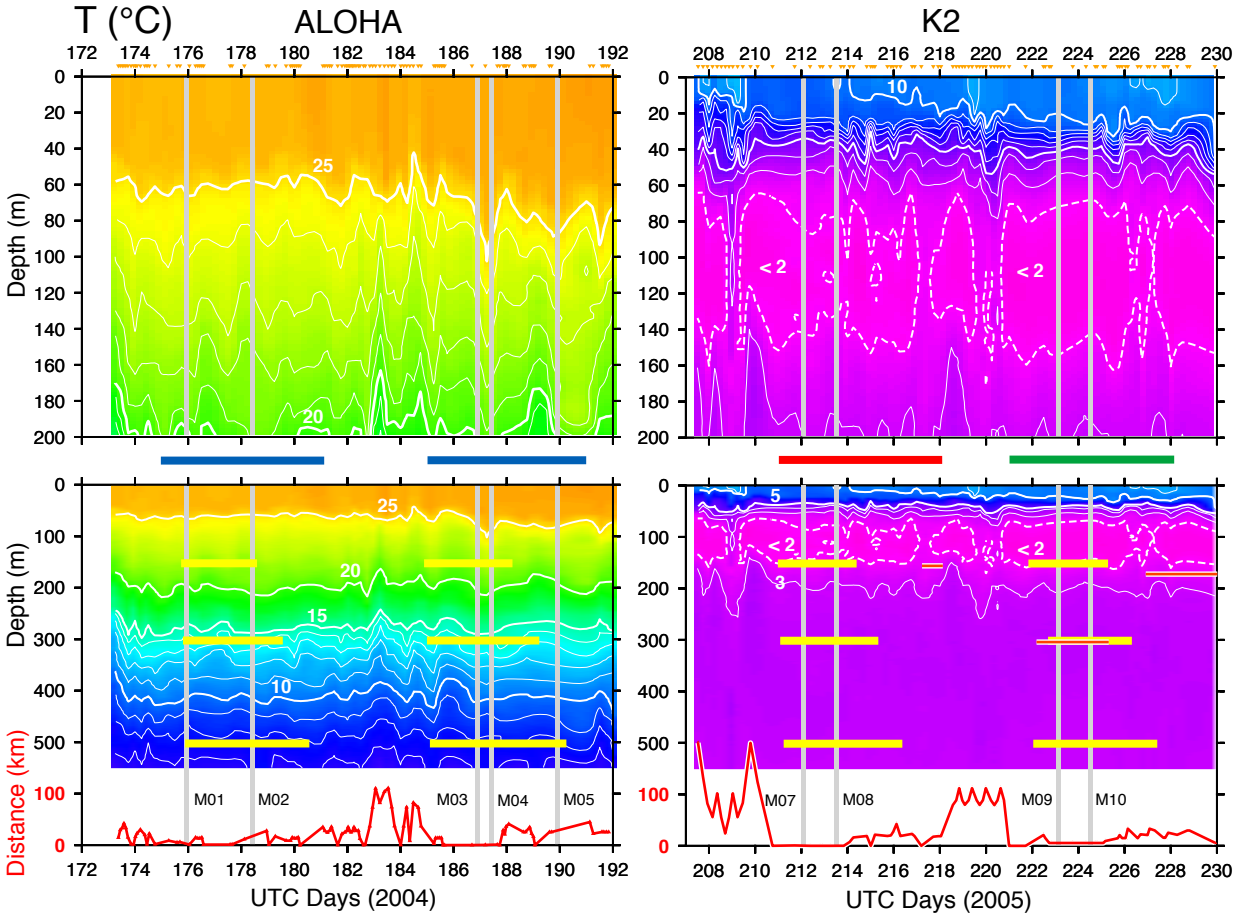
T (°C)
ALOHA
K2
Depth (m)
Distance (km)
UTC Days (2004)
UTC Days (2005)
M01
M02
M03
M04
M05
M07
M08
M09
M10
25
20
15
10
5
< 2
3

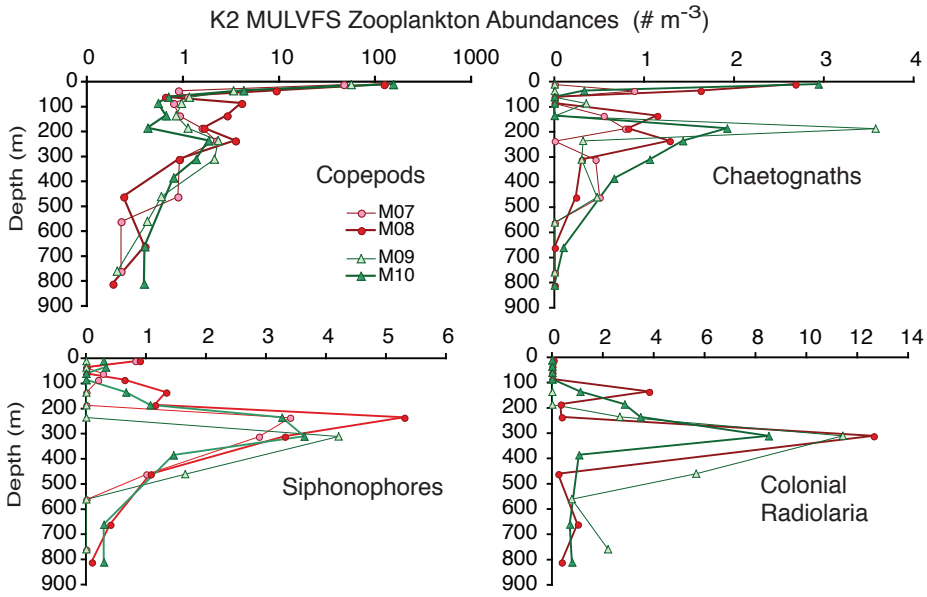
K2 MULVFS Zooplankton Abundances (# m-3)
Depth (m)
Copepods
M07
M08
M09
M10
Chaetognaths
Siphonophores
Colonial
Radiolaria

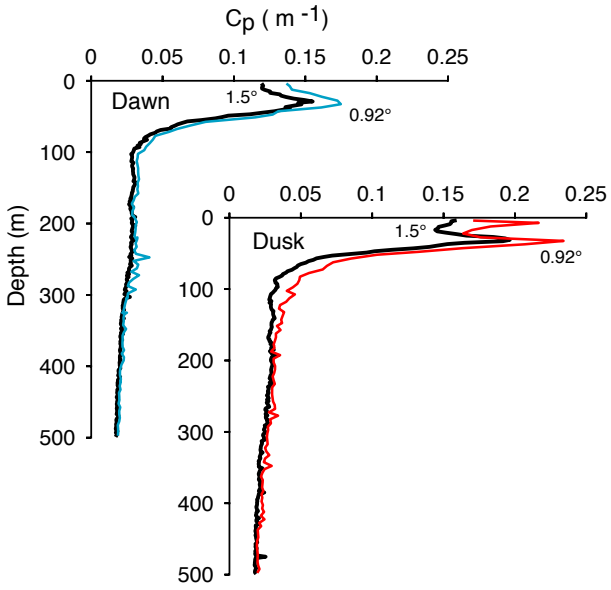
Cp (m -1)
0
0.05
0.1
0.15
0.2
0.25
Dawn
1.5°
0.92°
Dusk
Depth (m)
0
100
200
300
400
500

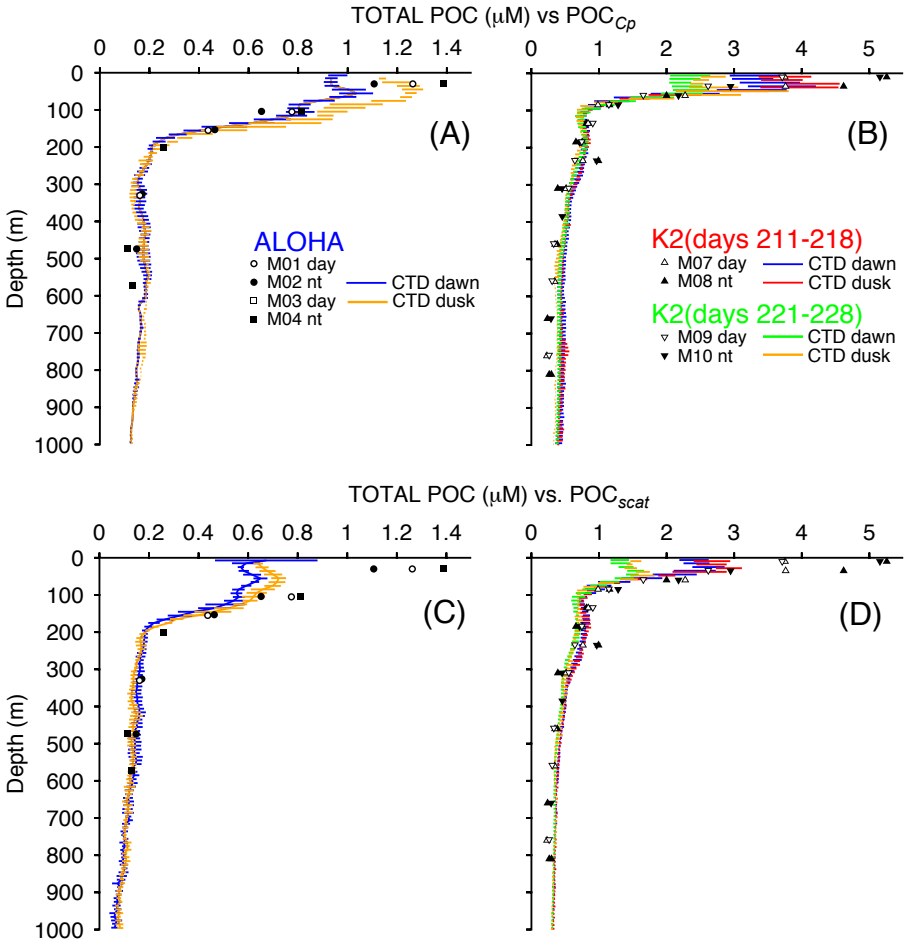
TOTAL POC (μM) vs POC$_{Cp}$
0 0.2 0.4 0.6 0.8 1 1.2 1.4
0 1 2 3 4 5
Depth (m)
0 100 200 300 400 500 600 700 800 900 1000
(A)
(B)
ALOHA
M01 day
M02 nt
M03 day
M04 nt
CTD dawn
CTD dusk
K2(days 211-218)
M07 day
M08 nt
CTD dawn
CTD dusk
K2(days 221-228)
M09 day
M10 nt
CTD dawn
CTD dusk
TOTAL POC (μM) vs. POC$_{scat}$
(C)
(D)

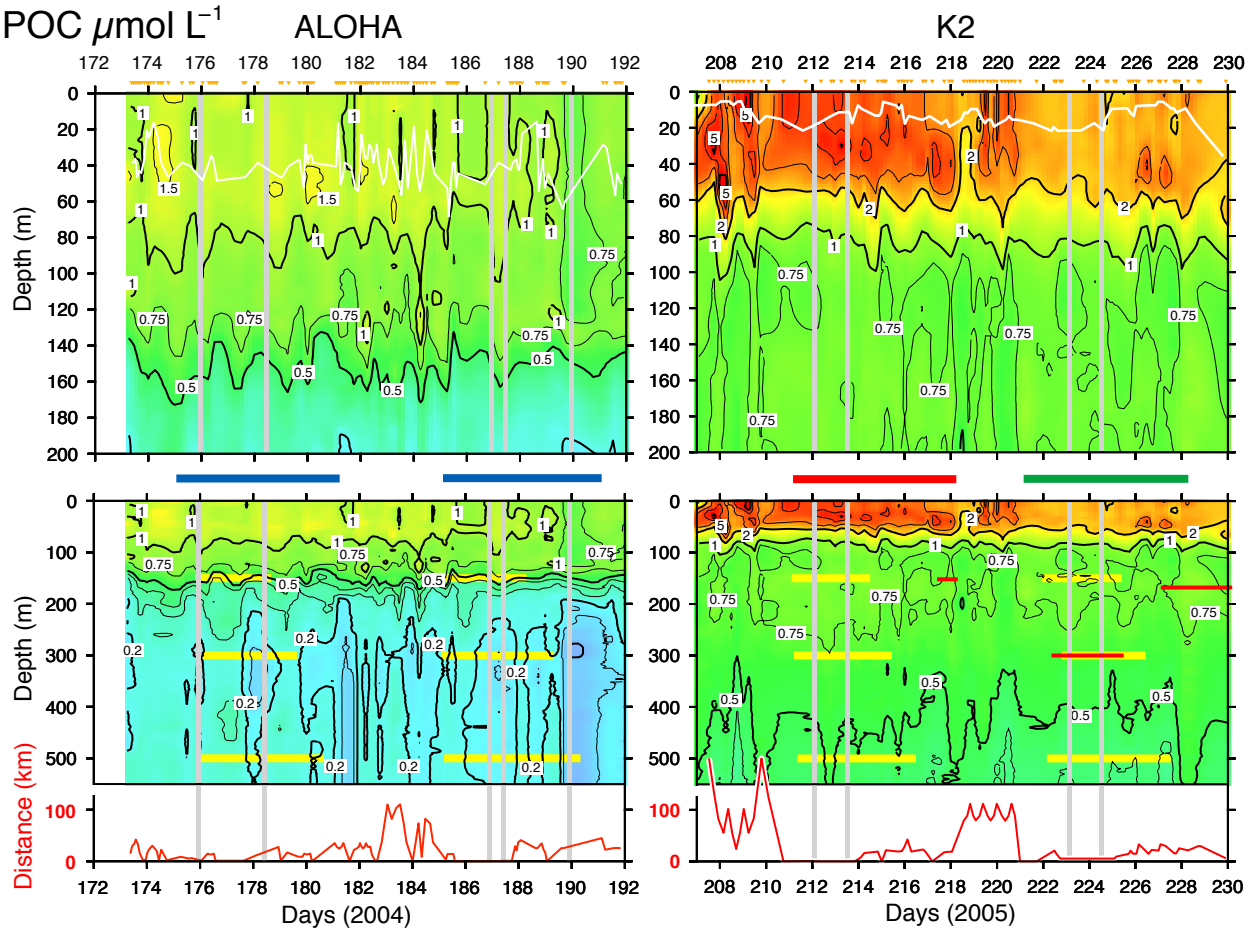
POC μmol L−1
ALOHA
K2
Depth (m)
Distance (km)
Days (2004)
Days (2005)

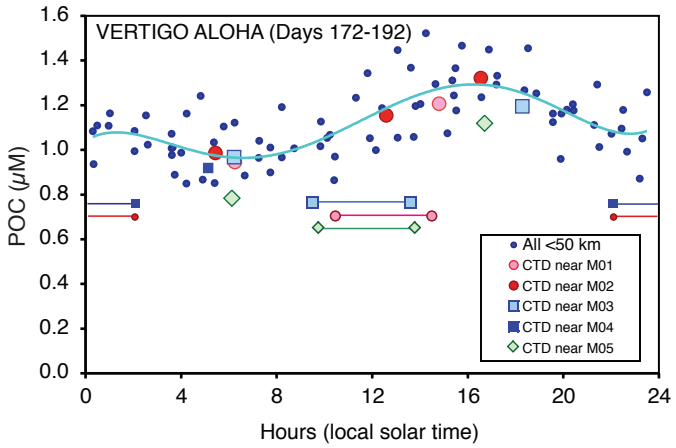
VERTIGO ALOHA (Days 172-192)
POC (μM)
1.6
1.4
1.2
1.0
0.8
0.6
0.4
0.2
0.0
0
4
8
12
16
20
24
Hours (local solar time)
All <50 km
CTD near M01
CTD near M02
CTD near M03
CTD near M04
CTD near M05

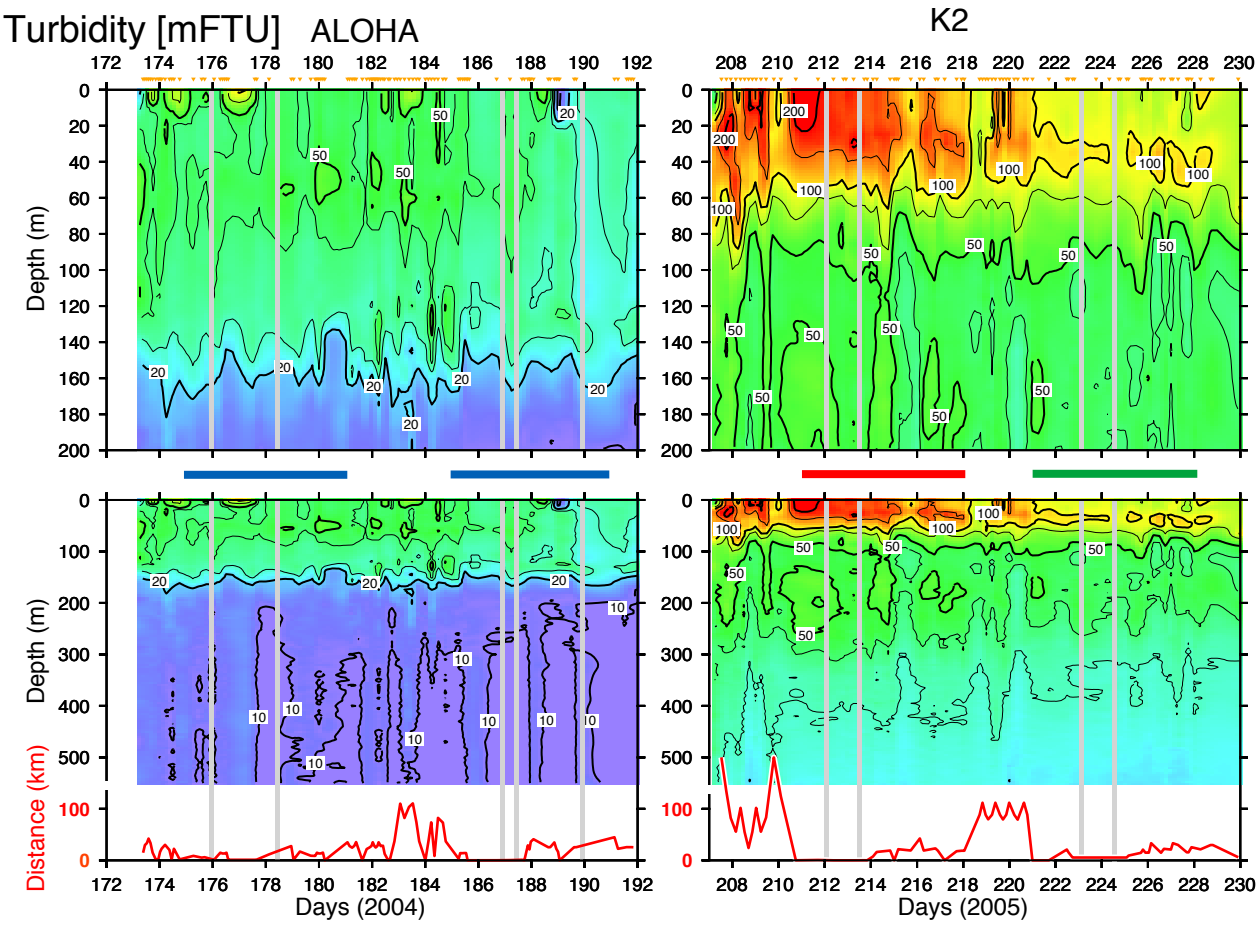
Turbidity [mFTU]
ALOHA
K2
Depth (m)
Distance (km)
Days (2004)
Days (2005)

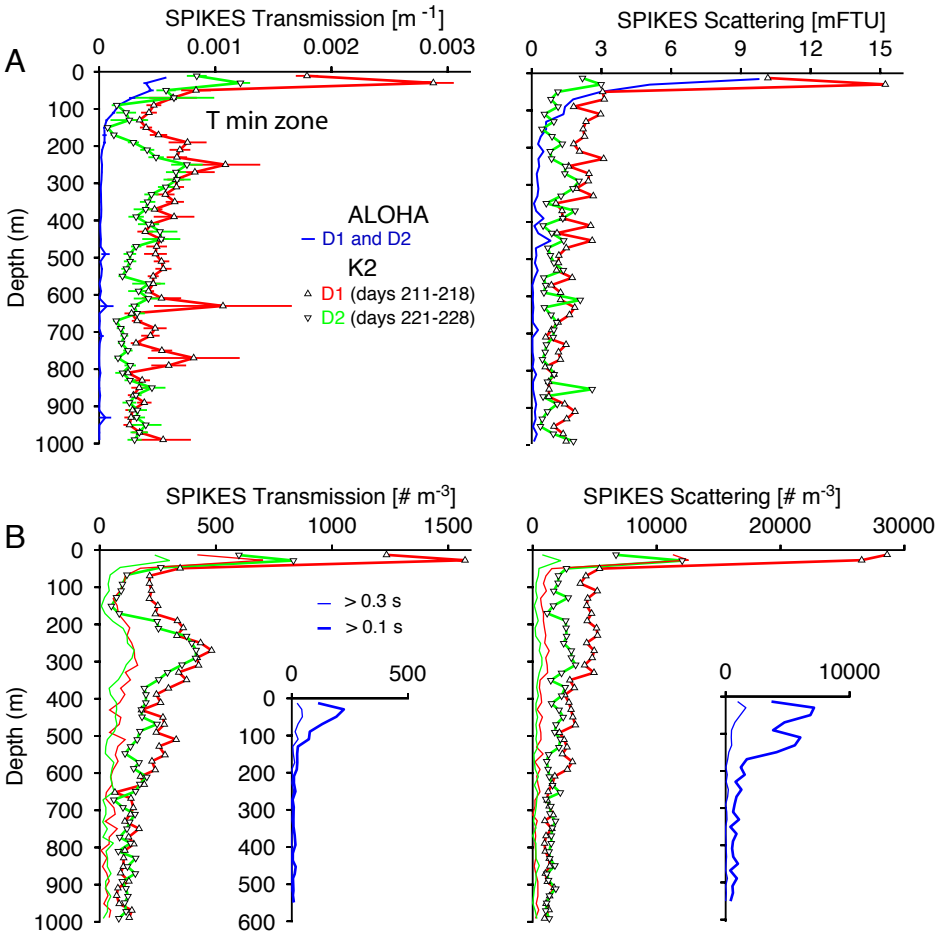
A
SPIKES Transmission [m -1]
0
0.001
0.002
0.003
SPIKES Scattering [mFTU]
0
3
6
9
12
15
Depth (m)
0
100
200
300
400
500
600
700
800
900
1000
T min zone
ALOHA
D1 and D2
K2
D1 (days 211-218)
D2 (days 221-228)
B
SPIKES Transmission [# m-3]
0
500
1000
1500
SPIKES Scattering [# m-3]
0
10000
20000
30000
> 0.3 s
> 0.1 s
0
500
0
10000
0
100
200
300
400
500
600

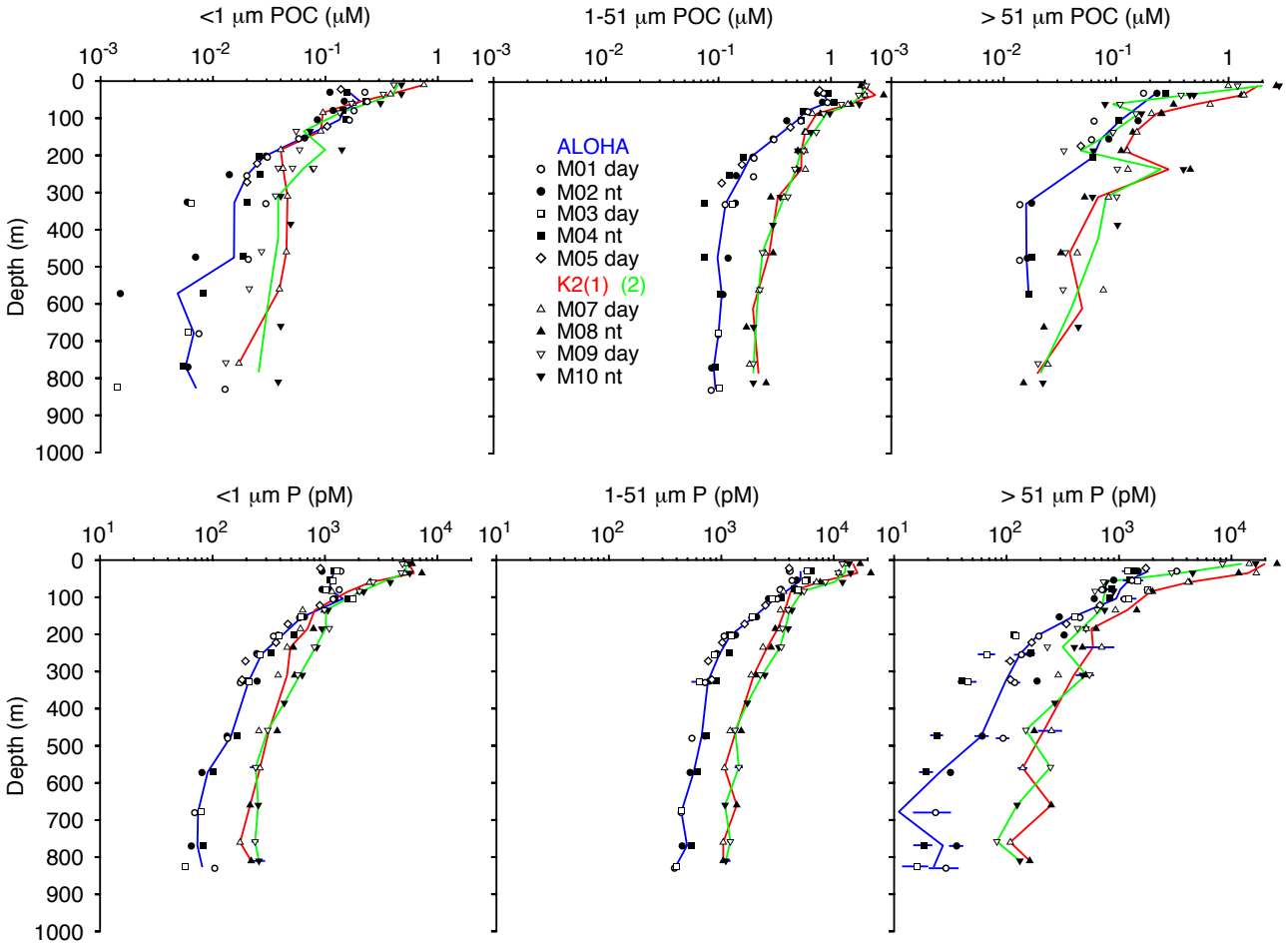
<1 μm POC (μM)
1-51 μm POC (μM)
> 51 μm POC (μM)
<1 μm P (pM)
1-51 μm P (pM)
> 51 μm P (pM)
Depth (m)
ALOHA
M01 day
M02 nt
M03 day
M04 nt
M05 day
K2(1) (2)
M07 day
M08 nt
M09 day
M10 nt

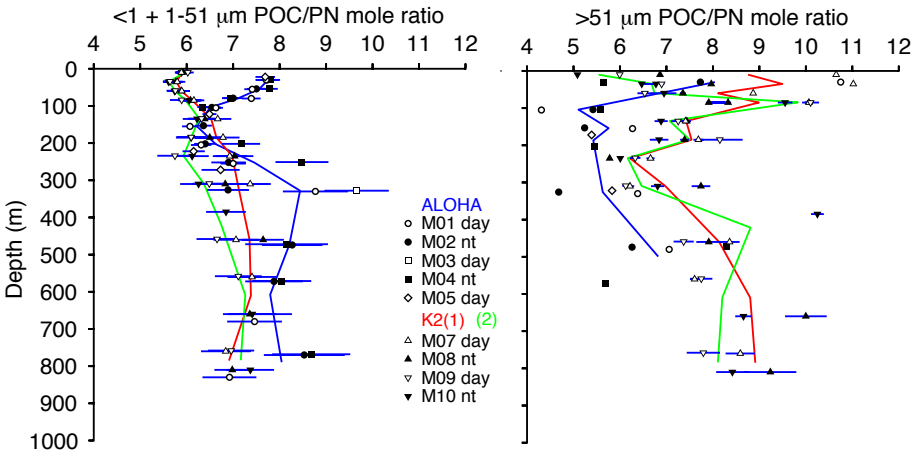
<1 + 1-51 μm POC/PN mole ratio
>51 μm POC/PN mole ratio
4 5 6 7 8 9 10 11 12
Depth (m)
0 100 200 300 400 500 600 700 800 900 1000
ALOHA
M01 day
M02 nt
M03 day
M04 nt
M05 day
K2(1) (2)
M07 day
M08 nt
M09 day
M10 nt

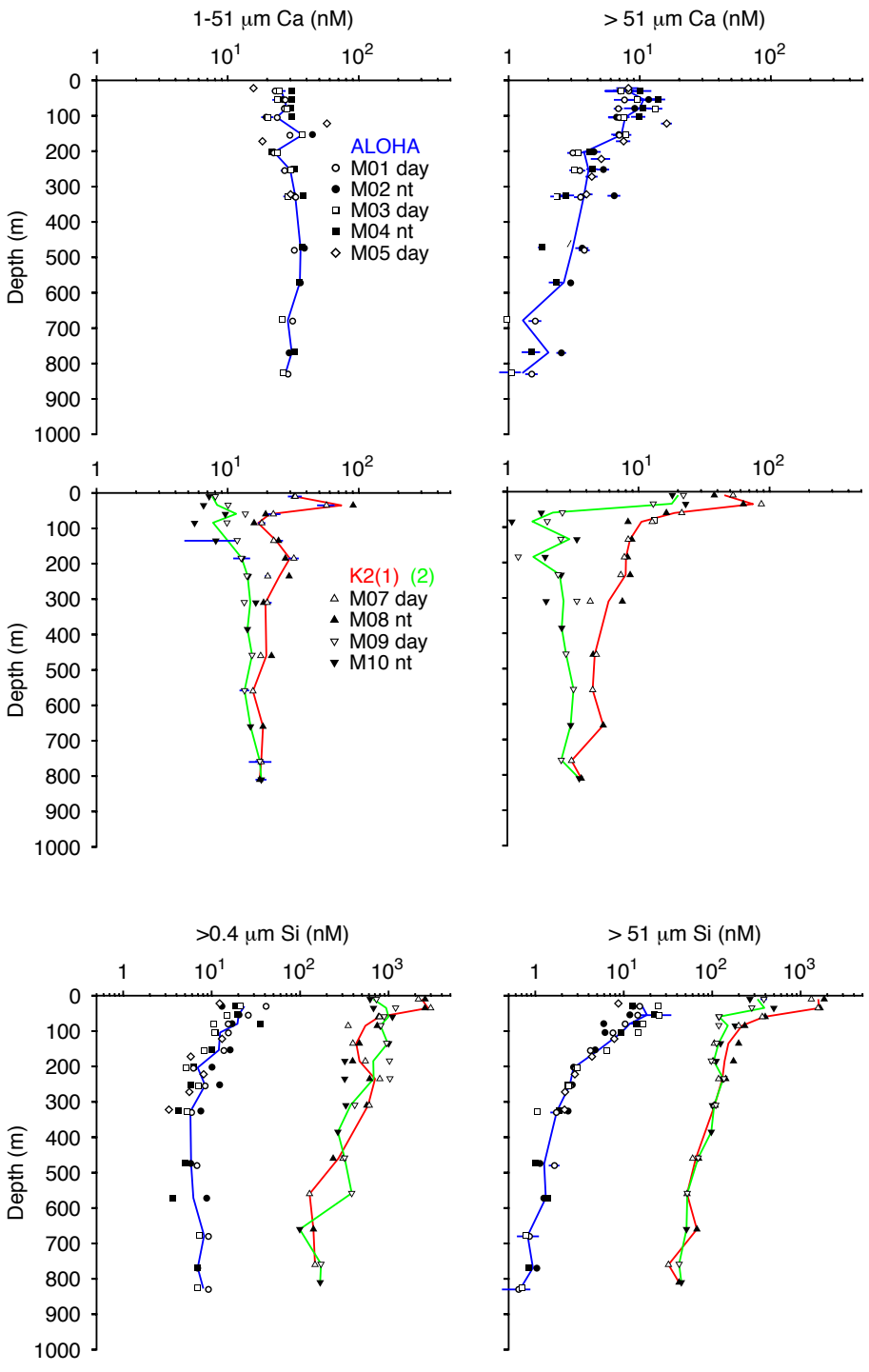
1-51 μm Ca (nM)
> 51 μm Ca (nM)
>0.4 μm Si (nM)
> 51 μm Si (nM)
Depth (m)
ALOHA
M01 day
M02 nt
M03 day
M04 nt
M05 day
K2(1) (2)
M07 day
M08 nt
M09 day
M10 nt

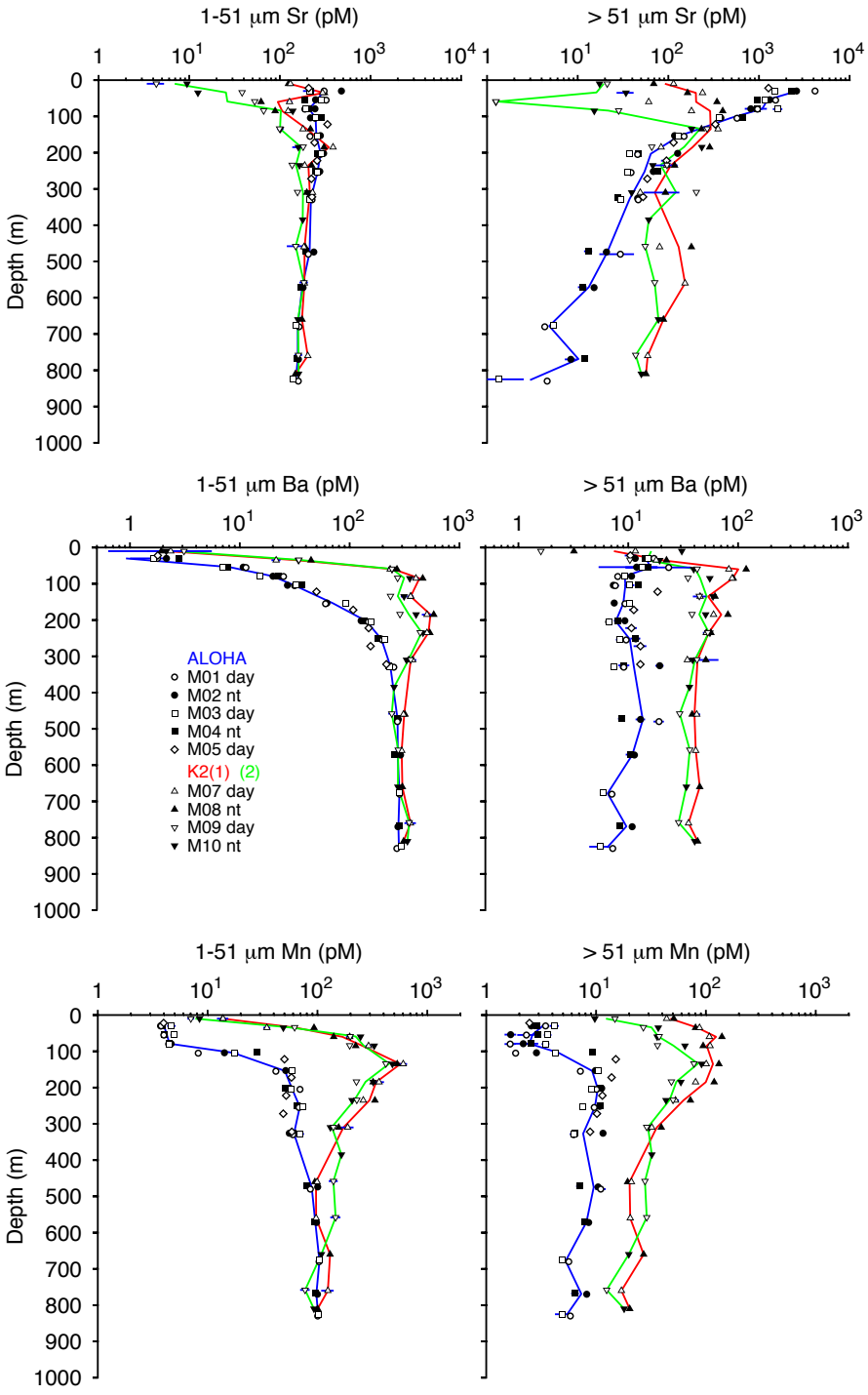
1-51 μm Sr (pM)
> 51 μm Sr (pM)
1-51 μm Ba (pM)
> 51 μm Ba (pM)
1-51 μm Mn (pM)
> 51 μm Mn (pM)
Depth (m)
ALOHA
M01 day
M02 nt
M03 day
M04 nt
M05 day
K2(1) (2)
M07 day
M08 nt
M09 day
M10 nt

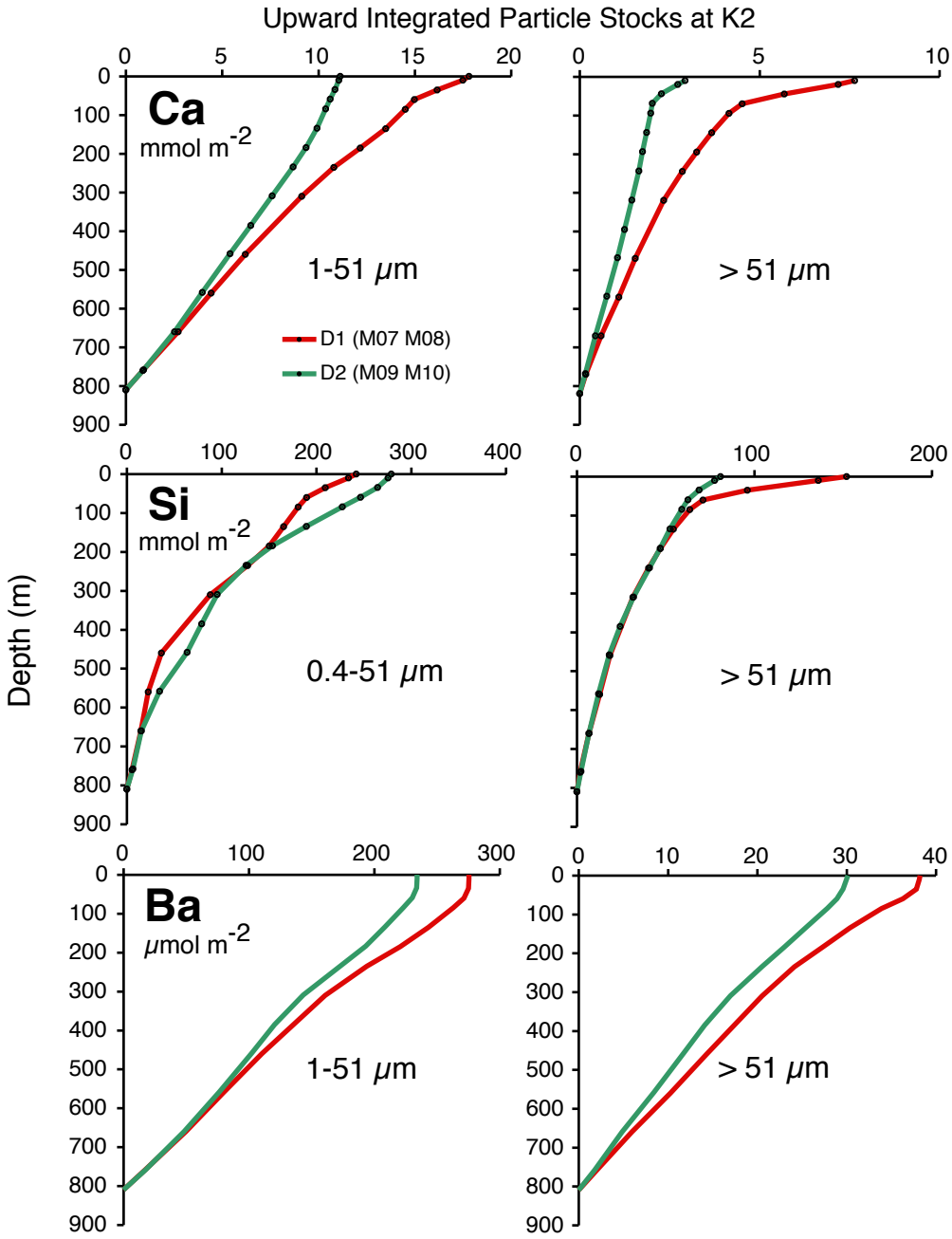
Upward Integrated Particle Stocks at K2
Depth (m)
Ca
mmol m-2
1-51 μm
> 51 μm
D1 (M07 M08)
D2 (M09 M10)
Si
mmol m-2
0.4-51 μm
> 51 μm
Ba
μmol m-2
1-51 μm
> 51 μm

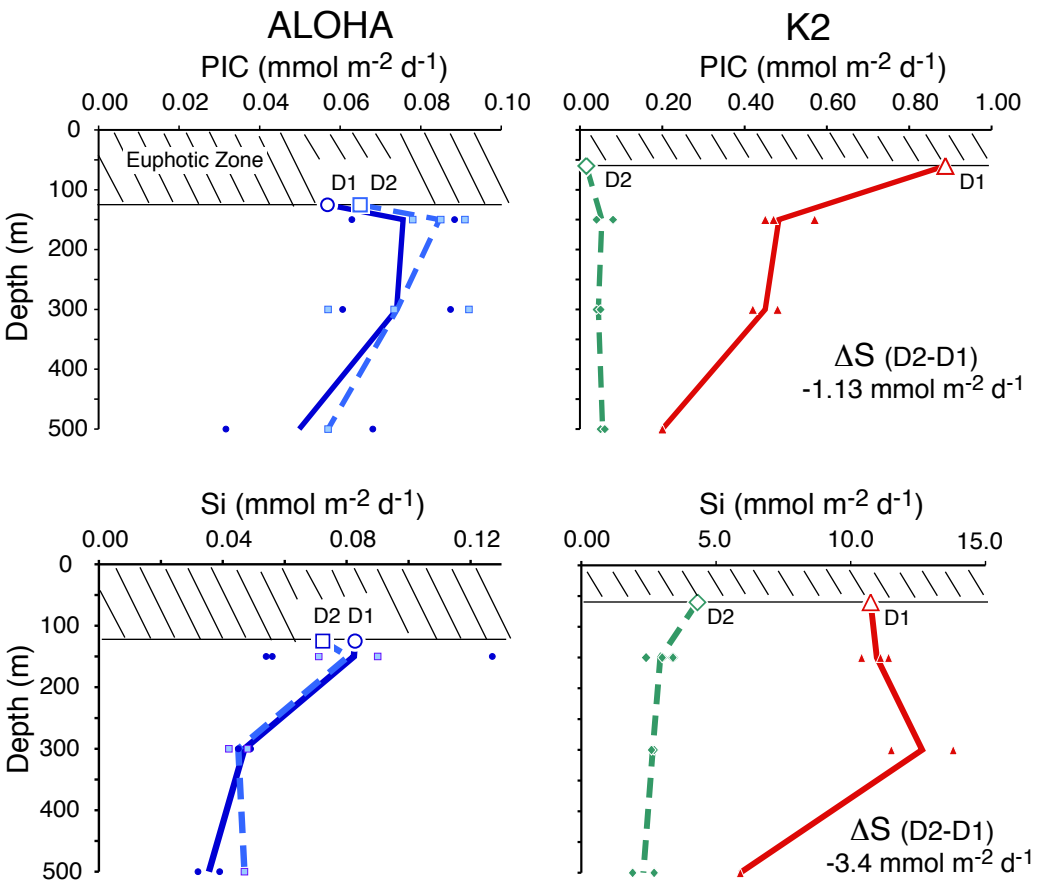
ALOHA
K2
PIC (mmol m-2 d-1)
PIC (mmol m-2 d-1)
0.00 0.02 0.04 0.06 0.08 0.10
0.00 0.20 0.40 0.60 0.80 1.00
Depth (m)
0
100
200
300
400
500
Euphotic Zone
D1 D2
D2
D1
ΔS (D2-D1)
-1.13 mmol m-2 d-1
Si (mmol m-2 d-1)
Si (mmol m-2 d-1)
0.00 0.04 0.08 0.12
0.00 5.0 10.0 15.0
D2 D1
D2
D1
ΔS (D2-D1)
-3.4 mmol m-2 d-1